This article has been accepted for publication in International Materials Reviews, published by Taylor & Francis.

Photocatalytic removal of model VOC pollutants: from a fundamental approach to real cases

Eleonora Pargoletti[a,b], Luca Rimoldi[a,b], Daniela Meroni[a,b,*], Giuseppe Cappelletti[a,b,*]

[a] *Dipartimento di Chimica, Università degli Studi di Milano, Milano, Italy*

[b] *Consorzio Interuniversitario Nazionale per la Scienza e la Tecnologia dei Materiali (INSTM), Florence, Italy*

** Corresponding author: giuseppe.cappelletti@unimi.it; daniela.meroni@unimi.it*

Abstract

The photocatalytic oxidation of volatile organic compounds (VOCs) has been extensively investigated. With respect to water treatment, photocatalytic degradation of air pollutants is still less understood, but this has not prevented photocatalytic building materials and air purifiers to reach the market. Here, we provide a selective overview of the current understanding on VOC photocatalytic oxidation, focusing on ethanol, acetaldehyde, and acetic acid. Among the main indoor pollutants, these molecules are also oxidation intermediates of numerous VOCs. Their adsorption at the photocatalyst surface is first presented, based on theoretical and experimental evidence. Reaction intermediates are discussed, comparing proposed reaction mechanisms. The role of the photocatalyst features in directing adsorption and oxidation phenomena is highlighted, encompassing both TiO_2 and emerging photocatalysts. We then critically discuss gaps in our knowledge, such as the effect of air humidity, multi-pollutant interactions and deactivation pathways. Finally, attempts to model VOC degradation in realistic conditions are reviewed.

Keywords

Pollutant remediation; titanium dioxide; air purifiers; air quality; household pollution; reaction pathway; photocatalytic oxidation; deactivation pathways.

Summary

1. Introduction

In recent years, indoor air quality has become a pressing concern[1] as people spend most of their time inside buildings (65-90%)[2,3]. A large number of air pollutants has been identified in households and offices, including numerous volatile organic compounds (VOCs), which derive from sources both inside buildings (consumer products, construction materials, tobacco smoke, etc) and outdoor surroundings[4,5]. Indoor environments can also increase the pollutant lifetime by slowing down the natural degradation processes, which are catalyzed by rain and sunlight[6]. As a result, pollutants concentrations in indoor air can be higher than those in the outdoor environment[7].

Among the various air pollutant remediation techniques, photocatalytic oxidation represents one of the most promising as it can degrade a broad range of pollutants (including some that are poorly removed by conventional remediation methods[8,9]), working in environmental conditions and without the addition of reagents[10–12]. Photocatalysis is based on the absorption of light of adequate wavelength by a semiconductor (photocatalyst), which elicits the excitation of electrons from the semiconductor valence band to its conduction band; the generated electron-hole pairs can either recombine or migrate to the surface of the photocatalyst, where they can promote redox reactions with adsorbed species[10]. The active material can be integrated in building materials and in air purifiers[13–15].

Despite the extensive literature results on this subject, the degradation of gas-phase pollutants is still less understood than photocatalysis in aqueous environment[16] and presents inherent unsolved problems. In gas-phase reactions, the photocatalyst deactivation issue is more pressing than in aqueous environment, where water can help to remove products and intermediates from the surface[17]. Other specific problems to overcome regard contact time, especially in high flow-rate systems, the role of air humidity, and adsorption competition among different species at the photocatalyst surface. The potential accumulation of toxic intermediates is another concern that demands an in-depth knowledge of the degradation mechanism.

This review article provides a critical overview of the adsorption and photocatalytic oxidation of selected VOCs: ethanol, acetaldehyde, and acetic acid, which represent key primary pollutants *per se*, emitted by both biogenic and anthropogenic sources (fermentations, biofuels, building materials and consumer products)[18,19]. Particularly, acetaldehyde is one of the main indoor pollutants due to its carcinogenicity and ubiquitous diffusion. Furthermore, these compounds are degradation intermediates of a wide range of pollutants like methylethylketone[20,21], acetone[22], toluene[23,24], ethyl acetate[25]. Owning to their relatively simple molecular structure (only two carbon atoms), they are often used as model molecules in both experimental and theoretical studies

for three broad classes of VOCs (alcohols, aldehydes, and carboxylic acids). In this respect, they represent better models than their one-carbon analogues due to the presence of C-C bonds, which make their chemistry more similar to that of longer hydrocarbon chains[26]. Finally, ethanol and acetaldehyde are widely used as model pollutants in laboratory settings to test the photocatalytic activity of new systems, due to their ease of detection and relatively fast photocatalytic degradation[27,28].

Hence, the present review focuses on their adsorption and degradation mechanism mainly on TiO_2-based photocatalysts, on the grounds of their large prevalence in literature reports and in currently available market technologies. The pollutant adsorption on TiO_2 photocatalysts will be first presented on the grounds of both theoretical and experimental evidence. The role of surface hydration/hydroxylation and competition between species will be discussed. In the second part, the reaction intermediates will be reviewed, with special emphasis on the role of oxygen and humidity. Then, the role of the photocatalyst features and modification strategies on the reaction kinetics and deactivation will be discussed, with reference not only to TiO_2 materials but also to other emerging photocatalysts. Finally, recent attempts to model VOC degradation in realistic conditions will be reviewed, discussing potential hurdles associated to byproducts accumulation. Fig.1 summarizes the main topics here covered.

2. Adsorption

Adsorption of ethanol, acetaldehyde and acetic acid has been extensively investigated both experimentally, by means of *in situ* Fourier Transform Infrared (FTIR) spectroscopy[29–33], Room Temperature Desorption, RTD[34], Temperature Programmed Desorption, TPD[34–37], Photoelectron Spectroscopy, PES[38–40], femtosecond two-Photon Photoemission spectroscopy, 2PPE[41], Nuclear Magnetic Resonance, NMR[42,43], and theoretically using *ab initio* calculations[44–47]. Scanning Tunneling Microscopy, STM, has also been employed to clarify the preferential pollutant adsorption sites[26,48–51].

In the following, the adsorption of each pollutant on dehydroxylated surfaces will be first reviewed. The role of surface hydration and presence of competing species will be then discussed.

2.1 Adsorption on dehydroxylated surfaces

2.1.1 Ethanol

Ethanol adsorption on TiO_2 surfaces has been studied extensively using STM[48–50], TPD[35,52], spectroscopic techniques[38,40], and density-functional theory (DFT) modeling[48–50,53].

Ethanol adsorption occurs preferentially in a dissociative way at temperatures >300 K, both on rutile(110)[38,44,48,52,54] and on anatase(101) TiO_2 surfaces[55]. In particular, ethanol dissociates at two-fold coordinated bridging oxygen (O_{br}) vacancies via O-H bond scission, leading to adsorbed ethoxide species bonded to the Ti^{3+} atom (*i.e.* with the oxygen atom of the former OH groups filling the O_{br} vacancy) and to the H adatoms capping a neighboring O_{br} atom (Fig.2). Theoretical calculations[44,48] showed an energy for this adsorption mode lower than that of the molecular one (Fig.2c,d). In this respect, photoemission studies on the band gap of TiO_2 rutile(110)–1×1 surfaces[40] showed that ethanol adsorption alters the surface charge associated with defects (*e.g.*, oxygen vacancies and Ti^{3+} interstitials): this observation supports attractive interactions between ethanol molecules and such defects (Fig.3).

Moreover, other adsorption geometries were also observed: STM experiments on rutile(110) surfaces provided direct evidence for the coexistence of dissociatively and molecularly adsorbed ethanol species on surface 5-fold coordinated Ti atoms, Ti_{5c}[48], in agreement with DFT calculations of adsorption energy on these sites[26,44,48]. Also in the case of anatase(101) surfaces, DFT calculations of adsorption geometries showed similar adsorption energies for the same adsorbed species[41,53,55]. Both adsorption modes on Ti_{5c} involve an interaction between a surface Ti_{5c} centre and the ethanol oxygen: the ethoxy species resulting from dissociative adsorption binds via a strong Ti-O bond with covalent and ionic character[48], whereas molecular adsorption gives rise to a weak bond via the oxygen lone pair, further stabilized by strong hydrogen-bonds[44]. Overall, ethanol acts as an electron donating adsorbate bound to the surface, hence responsible for a decrease in work function[44]. Even upon dissociative adsorption, ethanol retains its geometry, showing only a mild C–O shortening[44]. The molecular alignment of adsorbed ethanol has limited effect on the adsorption energy and on electronic states[44].

Molecular ethanol and ethoxide species can be distinguished in STM images due to their different apparent heights (Fig.2a,b) and diffusion rates. Time-lapse STM images showed the diffusion phenomena of ethanol molecules adsorbed at the surface[48,50]: molecularly adsorbed ethanol at Ti_{5c} sites can diffuse to other Ti_{5c} sites, unless it gets trapped at O_{br} vacancies where it dissociates forming an ethoxide species[48]. Conversely, dissociatively adsorbed ethanol cannot diffuse in the investigated temperature range (180-200 K)[48], as supported by calculated diffusion barrier energies[48]. FTIR spectroscopy studies confirmed this picture, as ethoxide species can be distinguished from molecular adsorption by the intense stretching band of C-O groups at *ca.* 1145 cm^{-1} and by the low intensity ratio of OH and CH bending bands[30].

TPD studies further supported the occurrence of a variety of adsorption modes[35,52,56]: desorption peaks up to 200 K are generally attributed to molecular adsorption[52], whereas those at

higher temperatures (up to 600 K) can be related to dissociative one[38,41,52,56]. Notably, dissociative adsorptions on Ti_{5c} sites and on oxygen vacancies were reported to give rise to separate TPD peaks (at *ca.* 370 K and >500 K, respectively)[52,56]. These attributions were confirmed by STM studies showing that, at low temperature (140 K) ethanol predominantly adsorbs at Ti_{5c} sites on rutile(110), whereas annealing at higher temperature favors adsorption at O_{br} sites; at T >380 K, only adsorption at O_{br} sites is appreciable[48]. TPD studies showed also a marked effect of ethanol coverage on the preferential adsorption mode, with dissociative adsorption favored at low coverage and molecular adsorption becoming prevalent at increasing ethanol dosage[52].Oxygen vacancies along step edges on rutile(110) were also reported to give rise to dissociative adsorption of ethanol[26,49,57]. A higher density of ethanol molecules was observed at the bottom of step edges on anatase(101), as opposed to upper step edges, and related to ethanol diffusion at room temperature, RT[55].

Ethanol displays a relatively weak adsorption in terms of mean sticking coefficient (0.03 on anatase(101) surfaces[55]), especially with respect to other molecules such as acetic acid (see Section 2.1.3), mirroring differences in adsorption energies. A maximum surface coverage of 50% was predicted theoretically[44] and observed experimentally[39,48]. STM images showed the coordination of ethanol in adjacent sites along the [010] direction of anatase(101) surfaces, with the C−C moiety oriented perpendicular to the titanium rows[55], similarly to acetic acid (see Section 2.1.3). This observation can be explained considering that the short side of the surface unit cell (∼3.7 Å) would prevent adsorption on two neighboring Ti cations.

2.1.2 Acetaldehyde

Also in the case of acetaldehyde adsorption on TiO_2 surfaces, a variety of adsorption modes (molecular, dissociative, and reactive ones) have been identified on the grounds of theoretical calculations and experimental evidence.

DFT studies showed that the most favored adsorption modes of acetaldehyde on rutile(110)[45] and anatase(101)[58] (the TiO_2 polymorphs' most stable surfaces) involve the interaction of the C=O dipole moment with the surface electric field due to Ti cations. In this respect, the rutile/anatase coverage ratio for acetaldehyde was reported to be 1.5[59], *i.e.* consistent with the difference in cation densities of the low-index surfaces of the two TiO_2 polymorphs[60]. In the case of stoichiometric and oxidized rutile surfaces, the most stable adsorption configuration is atop a Ti_{5c} channel site, which results in a distorted Ti-O bond and in an elongated C=O bond with respect to the pristine surface and free molecule, respectively, indicative of some adsorbate-to-surface charge transfer[45] (Fig.4a,b). Further stabilization of this geometry can arise from the hydrogen-bonding

interaction between the α-hydrogen and a lattice oxygen, due to the Brönsted acid character of the former. A similar adsorption mode was proposed also for anatase(001) surfaces[46]: in this case, Yao and coworkers[46] reported that the weakening of the carbonyl and Ti_{5c}-O_{br} bonds, ensuing the interaction between the carbonyl oxygen and Ti_{5c} sites, leads to the formation of a bond between the O_{br} and the C of the carbonyl group (Fig.5).

On the other hand, in reduced TiO_2 surfaces, a more energetically favorable adsorption configuration involves the insertion of the C=O into an oxygen vacancy with the acetaldehyde molecular symmetry plane parallel to the O_{br} row, as reported for rutile(110)[45] (Fig.4b). Also in this case, the α-hydrogen atom of acetaldehyde molecules is tilted towards a nearby lattice oxygen. This stabilizing interaction imposes an energy barrier to acetaldehyde molecule diffusion along the oxygen row, which is however easily overcome at RT by passing through a bidentate configuration with a bridging oxygen atom. DFT calculations showed that adsorption on reduced surfaces is energetically slightly more favored than that on stoichiometric surfaces[45], as also confirmed by TPD experiments[32].

TPD studies in ultra-high vacuum, UHV, of reduced and oxidized rutile(110)[36] showed a coverage dependence in acetaldehyde binding energy, even at low coverage (<0.5 monolayer coverage, ML). This effect is more significant for the low temperature component, assigned to acetaldehyde bond with Ti_{5c} sites, which shifts towards lower energy at increasing surface coverage. This effect can be ascribed to dipole-dipole repulsions between co-adsorbed acetaldehyde molecules and to a reduction in the acidity of neighboring Ti_{5c} sites, due to charge transfer effects upon acetaldehyde bonding.

FTIR studies confirmed the formation of different adsorption modes of acetaldehyde at TiO_2 surfaces as different peaks, attributable to carbonyl stretching, can be observed at *ca.* 1710 and 1690 cm^{-1}[29,32,58], also fully in agreement with TPD results[34]. The red shift of these bands with respect to gas-phase spectra (where $\nu_{C=O}$ occurs at *ca.* 1750 cm^{-1}) indicates an adsorption mechanism via coordination of the carbonyl oxygen to the surface. The peak at *ca.* 1710 cm^{-1} is generally attributed to a poorly stable molecular adsorption mode due to H-bonding with surface hydroxyls, as also supported by the increase in the broad band around 3400 cm^{-1} ascribable to H-bonded OH groups[32,61]. On the other hand, the most shifted carbonyl stretching is attributed to a more stable adsorption mode involving a covalent bond between the carbonyl oxygen and Lewis acid sites at the TiO_2 surface (Ti_{5c} centers)[32,58,61]. While the irreversible adsorption mode is not impacted by surface hydroxylation, the fraction of reversibly bound acetaldehyde molecules depends on the density of surface hydroxyls[34,61]. In particular, at low surface hydroxylation, the reversible adsorption is almost negligible[34,59,62], as confirmed by DFT studies.

Reactive adsorption at RT has also been consistently reported for acetaldehyde adsorption on a series of oxides, including TiO_2[32]. Besides acetaldehyde bands, FTIR spectra on TiO_2 present additional peaks at *ca.* 1660, 1630 and 1160 cm^{-1}, showing intensity increasing with time at the expense of the peaks of acetaldehyde carbonyl. These peaks are generally attributed to the stretching modes of C=O, C=C and C-C of crotonaldehyde[32,58,59,61,63], respectively. Adsorption of acetaldehyde on TiO_2 at RT was reported to produce crotonaldehyde via aldol condensation[29,32,42,58,61,63,64] and, as short-lived intermediate, 3-hydroxybutanal[29,61]. Aldol condensation of adsorbed acetaldehyde molecules is catalyzed by nearby lattice oxygens, acting as Lewis base sites for abstraction of α-hydrogen[64] (Fig.6). As a result, this reaction is favored in extensively oxidized surfaces. Aldol condensation of acetaldehyde was reported on rutile at 313 K[59], on anatase at 373 K[59], and on brookite nanorods at 460 K[37], indicative of a lower activation energy for aldolization on rutile. Crotonaldehyde formation was observed on mixed TiO_2 phases also at lower temperatures (down to 251 K), although with slow kinetics[61]. Further aldolization producing higher-molecular-weight species was reported [32,65,66]. Reduced surfaces favor, instead, the formation of butene by reductive coupling of acetaldehyde at high temperature[36,64,67].

Lower fractions of acetate species[29,32,36,61] and ethoxide species[32] were also reported upon adsorption of acetaldehyde on TiO_2 at RT. Acetate formation was reported to occur preferably on oxidized surfaces[36] and was attributed to oxidation reactions between an adsorbed acetaldehyde molecule and an oxygen adatom followed by deprotonation, which result in a bidentate acetate on the Ti_{5c} channel and in an hydroxyl on the O row[45] (Fig.3).

2.1.3 Acetic acid

The adsorption of carboxylic acids at TiO_2 surfaces has been investigated extensively, owing to the bonding stability, which enables the formation of self-assembled monolayers and the use of carboxylic acids as organic linkers for dye molecules in solar cells[68,69]. As other carboxylic acids, acetic acid generally adsorbs via dissociative chemisorption in a bidentate bridging mode, where the two carboxylate oxygens coordinate to two neighboring Ti_{5c} atoms, whereas the acetic hydrogen adsorbs on O_{br}[51,70–77]. Both experimental[51,77] and theoretical studies[47,69,78,79] show no molecularly adsorbed acetic acid at RT on dehydroxylated surfaces. (110)Rutile, (101) and (001) anatase facets present bidentate bridging adsorption[51,74,77] (Fig.7), despite the increased separation of the Ti_{5c} sites on anatase(101) (3.78 Å) with respect to rutile(110) (2.96 Å), which could result in an increased strain of the binding[77]. Moreover, acetic acid was reported to adsorb dissociatively in a bridging configuration also on brookite[37]. Indeed, theoretical calculations

showed that bidentate configurations have the lowest-energy adsorption energies for dehydroxylated surfaces of the most stable crystal planes of anatase, brookite and rutile[47]. Acetic acid has a strong interaction with both anatase and rutile, with a near unity sticking probability for both anatase(101) and rutile(110) surfaces[51,77] and the adsorption mode is not affected by the coverage degree[51,77]. STM studies showed that, at variance with ethanol (see Section 2.1.1), acetate adsorbs homogenously on both rutile(110) and anatase(110)[51,77], with no apparent preference for defect sites, like step edges. However, differences between the two surfaces were reported in terms of the adsorbed acetate mobility at RT and ordering at high coverage[51,77,80]. In rutile(110), a bidentate coordination occurs between adjacent Ti_{5c} sites along the rows in the [001] direction, leading to an ordered (2×1) acetate overlayer at saturation coverage (corresponding to 0.5 ML)[51,81], whereas no long range ordering of the adsorbate at saturation coverage was observed for anatase(110) at RT[77] (Fig.8).

The adsorption geometry was reported to vary with the crystal planes involved. Other crystal planes, such as rutile(011)–2×1 surfaces, display a monodentate coordination[51]. Moreover, STM studies showed that initially acetate adsorbs only at surface defects of this surface, as the adsorption at the Ti_{5c} sites is sterically hindered by the coordination of protruding O_{2c} lattice oxygens[51]. A self-catalyzed adsorption mechanism was observed: the pre-adsorbed acetic acid facilitates the adsorption of further acetic acid molecules along these nucleated acetate clusters, which then spread to the defect-free terraces[51].

2.2 Adsorption competition with other species

Most studies about VOC adsorption on TiO_2 investigated fresh photocatalyst surfaces, *i.e.* in the absence of other species competing for adsorption. However, real effluents present complex mixtures of various pollutants and concurrent adsorption can occur among the different species. Competition phenomena can be limited for low pollutant concentrations (ppbv), but more significant at ppmv levels[82].

As acetic acid and acetaldehyde are intermediates during the photocatalytic degradation of ethanol, their possible competition for adsorption at the TiO_2 surface is particularly relevant. It was shown that acetic acid displaces acetaldehyde[34] and alcohols[33]. These observations are also supported by TPD data on rutile and brookite TiO_2: while acetic acid shows substantial thermal desorption at high temperature ($T >> 300$ K)[37,81], most of acetaldehyde desorbs molecularly[36,37] at $T < 300$ K[37,57,83]. Moreover, acetaldehyde and crotonaldehyde adsorb in a similar way on both anatase and rutile, and either aldehydes could displace the other from the surface layer[59]. On the contrary, a significant fraction of ethanol desorbs at $T > 300$ K, in particular when molecules adsorb

dissociatively as ethoxide species[38,41,52,56]. At comparable surface coverage, acetaldehyde is thus thermally desorbed at lower temperature than ethanol[41]. DFT calculations of adsorption energies of ethanol and acetaldehyde[57] further support this picture and can help to rationalize the concentration profiles of reaction intermediates during ethanol photocatalytic degradation: particularly, it is generally observed that acetaldehyde concentration builds up until ethanol has completely disappeared, while acetic acid is only observed at the photocatalyst surface[18,84,85] (see Section 3.1.1).

Few reports investigated the interaction between our model VOCs and other air pollutants. Thevenet and coauthors[62] studied the competition for adsorption between acetaldehyde and ubiquitous air pollutants, nitrogen oxides. NO_x are characterized by reactive adsorption properties at TiO_2 surfaces, leading to irreversibly adsorbed species[86]. Both reversibly and irreversibly adsorbed fractions of acetaldehyde are negatively impacted by the pre-adsorption of NO_x[62] (Fig.9). Several mechanisms seem to be at play beside competitive adsorption. The loss of reversible adsorption can be due to a lower surface hydroxylation ensuing NO_x adsorption; adsorbed NO_2 and/or NO_x are known to increase the TiO_2 surface acidity by consuming surface hydroxyls[87]. Moreover, adsorbed NO_x^- species modify the TiO_2 surface chemistry and acetaldehyde reactive adsorption, possibly leading to the formation of a new adsorption mode[62].

2.3 Effect of surface hydroxylation and hydration

While numerous theoretical and experimental adsorption studies considered dehydrated and dehydroxylated surfaces (*e.g.*, STM and PES studies are performed in UHV after thorough surface cleaning, often by ion sputtering), in real applications the TiO_2 surface is hydroxylated and covered by layers of water molecules. As water can block adsorption at defect sites[88], the oxide surface in environmental condition is less prone to adsorb pollutants, hence the formation of some of the reported adsorption products (*e.g.*, alkoxydes and carboxylates) may occur only on dry surfaces[82]. Pichat[82] suggested that organic pollutants, especially in ppbv concentrations, remain undissociated in the adsorbed water layers until reaction with the active species. Indeed, although the adsorption of acetic acid is much stronger than that of water[33], recent studies showed a variation in the adsorption modes of acetic acid on anatase in humid conditions from a dissociative chemisorption (bridged bidentate acetate) to a molecular chemisorption (monodentate-coordination)[89]. In the latter, the acetic acid molecules are bonded at Lewis acid sites (Ti^{4+}) and form hydrogen-bonds with neighboring water or acetic acid adsorbed molecules (Fig.10)[90,91]. This variation in adsorption geometry was reported also for formic acid[92]. The monodentate mode yields a characteristic FTIR carbonyl peak at *ca.* 1675 cm^{-1}, often reported at RT in surfaces

with residual hydroxylation[90,91]. The parallel occurrence of simple adsorption of acetic acid molecules via mere hydrogen-bonding has been scarcely reported[91,93] on the grounds of a weak FTIR signal at 1736 cm^{-1}. It is worth noting that in dry conditions, dissociative chemisorption (bidentate acetate, showing characteristic –COO– antisymmetric and symmetric stretching frequencies at *ca.* 1540 and 1450 cm^{-1}[89–91]) is largely prevailing over reversible molecular adsorption, especially at low coverage[89], as shown by RTD experiments[34,94]. Humid conditions markedly increase the amount of reversibly adsorbed acetic acid at the TiO_2 surface, which, however, still remains in equilibrium with chemisorbed acetate species[34,91,94].

Batault *et al.*[34] investigated the impact of humidity on acetaldehyde and acetic acid adsorption on TiO_2: they found considerable differences between the two VOCs, which are directly related to their adsorption modes and to the VOC–water interactions in adsorbed phase, related in their turn to the pollutant hydrophilicity. In humid conditions (RH=50%), acetaldehyde adsorption is completely reversible[34], whereas both adsorption modes of acetic acid are in equilibrium. Notably, in the absence of surface hydroxylation, the reversible adsorption of acetaldehyde is almost negligible with respect to the irreversible modes[34,59,62]. Similarly, the adsorption on anatase of another low weight aliphatic alcohol, methanol, gives rise to the formation of methoxy groups only below 10 Torr of water vapor pressure[33].

Water vapor affects not only the adsorption mode of acetaldehyde and ethanol, but also the total adsorbed amount. In particular, water molecules can displace ethanol and acetaldehyde from the TiO_2 surface, hence the adsorbed amount of these two pollutants decreases significantly in humid conditions[34,95,96], which has significant consequences in terms of reaction kinetics (see Section 3.3).

3. Reaction mechanism

3.1 Reaction intermediates

The reaction intermediates of ethanol, acetaldehyde, and acetic acid have been identified mainly using gas chromatography[85,94,97], mass spectrometry[35,55,94,98], TPD[36,83,88,99] and FTIR spectroscopy[29,30,63,89,91]. The reaction mechanism has been corroborated also via isotope labeling studies[36,90,94,100], NMR[42,43,101], electron spin resonance spectroscopy, ESR[102], STM[26,57], photon stimulated desorption, PSD[36,99], 2PPE[41] and DFT calculations[26,44,89]. In the following, the reaction mechanism of each pollutant will be discussed separately. The role of oxygen and water on the photocatalytic pathway will then be presented.

3.1.1 Ethanol

Among the three pollutants this review is focused on, the photocatalytic degradation pathway of ethanol has received the most attention, partly motivated by ethanol potential for H_2 production using metal-modified TiO_2[103]. The main intermediate in ethanol photocatalytic oxidation is acetaldehyde. Acetaldehyde formation is widely regarded as the initial step of ethanol oxidation[29,104] (Fig.11). Only few alternatives have been proposed: Pilkenton and coauthors[43] suggested that acetaldehyde is produced from the oxidation of a different first intermediate, 1,1-diethoxyethane. The pathway of acetaldehyde degradation is instead much more debated. Besides acetaldehyde, other commonly observed intermediates are adsorbed acetate and formate species together with their corresponding acids, as supported by GC[105], FTIR[30,106–108], STM[55] and XPS studies[39,55]. Formate/acetate species are thought to form via reaction of acetaldehyde with oxygen-containing radicals[55,56], as discussed in Section 3.2. Few authors reported also traces of condensation products, such as ethyl acetate, methyl acetate and methyl formate[105,109].

The first step of ethanol photocatalytic oxidation was investigated in single-crystal studies under UHV conditions: a hydrogen atom is removed from the α-carbon (*i.e.*, the carbon of the functional group, $-CH_2OH$) of either ethoxide groups or molecularly adsorbed ethanol, giving rise to adsorbed acetaldehyde and an adsorbed water molecule by reaction between the abstracted hydrogen and a surface hydroxyl group[26]. The same reaction was for both reduced and oxidized rutile(110)[88] and anatase(101)[55] surfaces, and was supported by DFT calculations[26] (Fig.12).

A 2PPE study reported the initial formation of a photo-induced excited state at ~2.4 eV above the Fermi energy during the photocatalytic degradation of ethanol over rutile(110), which was related to bridging hydroxyls forming hydrogen bonds with dissociated ethanol adsorbed on Ti_{5f} sites[41], similarly to previous reports on methanol[110].

The α-hydrogen elimination reaction is a hole mediated process[88]. Surface adsorbed alcohols are generally regarded as hole-trap molecules, able to transfer an electron to a hole in the valence band of the semiconductor[44,106,111]. Tamaki *et al.*[111] observed electron transfer from trapped holes in TiO_2 to alcohol molecules by transient absorption spectroscopy: the process is faster for methanol (~100 ps), but occurs in the ns scale for both ethanol and isopropanol (*ca.* 1 ns and 3 ns, respectively). When the adsorbed ethanol is converted to acetaldehyde, there is an overall electronic transfer of two electrons from the ethoxide to TiO_2 states[26]: one electron is captured by the photo-generated hole (hole trapping), *i.e.* it is transferred to the top of the TiO_2 valence band, while the other is directly transferred to the conduction band (insets of Fig.12b,c) as the radical species generated by the hole trapping step ($CH_3CH^{\bullet}O$) has sufficient energy (current doubling mechanism[57,112]).

Both ethoxide species and adsorbed molecular ethanol can act as hole traps thanks to their oxygen lone pairs[44]: DOS calculations showed that photogenerated charges migrated to the bound Ti can be trapped by ethanol states associated with the oxygen lone pairs[44]. This is in agreement with STM studies showing that regular Ti surface sites are the most active sites in the photocatalytic oxidation reactions on reduced rutile(110) surfaces[26]. As the energy difference between the ethanol highest occupied molecular orbital (HOMO) and the Ti highest occupied electronic state is almost the same for molecularly and dissociatively adsorbed ethanol, both adsorption modes are expected to display a similar trapping efficiency[44]. However, ethoxide species were reported to photo-oxidize faster than molecularly adsorbed ethanol[101], with similar observations for methanol/methoxide groups[113], possibly as the dissociatively adsorbed ethanol has more states which could act as electron traps due to its additional lone pair.

The involved reactive species may vary depending on the reaction conditions, such as surface coverage. Yu *et al.*[106] reported hole-initiated oxidation at high ethanol coverage, as the surface is deficient in adsorbed water, whereas at low ethanol coverage a main role of hydroxyl radical was suggested on the grounds of *in situ* IR studies.

The presence of active sites with different reaction mechanism has been hypothesized also on the grounds of kinetics studies[105,114]. Recently, Hansen and coauthors observed diverse reaction rates for ethanol molecules bound to Ti_{5c} sites, O_{br} vacancies and oxygen defects at step edges[26], with molecules bound to oxygen vacancies reacting only in the presence of O_2 and with more difficulty in step edges.

The second step of ethanol photocatalytic oxidation can involve the photooxidation of aldehyde by hole capture, leading to methyl radicals and surface-bound carboxylate species (in particular adsorbed formate species[57]), as shown by pump–probe laser ionization studies[83]. This conclusion is also supported by isotopic labeling investigations[114–116], showing that the CO_2 evolved in the first reaction stages comes from conversion of the α-carbon. Similar observations were reported for the degradation of acetaldehyde and acetic acid, as extensively discussed in the following sections (see 3.1.2-3.1.3), supporting a common surface intermediate before C–C bond cleavage.

3.1.2 Acetaldehyde

The degradation of acetaldehyde has been mostly studied as an intermediate in ethanol degradation[85,105,114], but few studies are devoted specifically to acetaldehyde degradation[29,42,63,107]. There is no consensus on the reaction mechanism of acetaldehyde photocatalytic oxidation on TiO_2. Its degradation was proposed to give rise directly to

CO_2[84,117,118], in particular when the amount of incident photons exceeds the adsorbed acetaldehyde molecules. On the other hand, the formation of several intermediates was reported by several authors: acetic acid/acetate[117], formaldehyde[29,105], formic acid/formate[63,119], together with condensation products, such as ethyl acetate, methyl formate and ethyl formate[105].

The occurrence of several parallel reaction pathways has been consistently reported by several authors. Using isotopic labeling, Muggli *et al.*[114] proposed two parallel pathways for the photodegradation of acetaldehyde on TiO_2, one involving acetic acid and the other one only formate intermediates. The former involves the direct formation of acetic acid from acetaldehyde, and the subsequent oxidation of its α-carbon directly to CO_2, while the β-carbon produces formate intermediates, before being oxidized to CO_2. The latter instead gives rise directly to a formic acid/formaldehyde mixture, which is then further oxidized to CO_2. Evidence of the latter pathway was reported by Zehr and coworkers[36], who investigated the acetaldehyde degradation mechanism on a dehydroxylated, reduced rutile(110) surface in the presence of O_2. They found that, in those experimental conditions, acetaldehyde undergoes a facile thermal reaction to produce an acetaldehyde-oxygen complex (estimated activation energy *ca.* 8 kJ mol^{-1}). Upon UV light irradiation, this complex ejects a $CH_3^{\bullet}$ radical into gas-phase upon cleavage of the C-C bond[120]; methyl radicals can be expected to be re-adsorbed on the surface to form methoxy groups, which are then converted to formate species[29]. The surface bound fragment deriving from the α-carbon is instead directly converted to adsorbed formate species. PSD studies showed the complex degradation is mediated by photogenerated charge carriers from the TiO_2 substrate rather than direct photon absorption by the adsorbate[36]. Similar conclusions were reached by Wilson and coauthors for a broader range of carbonyl containing compounds, including acetaldehyde[120]. The occurrence of a parallel reaction pathway on reduced TiO_2 surfaces was also suggested by Xu and coauthors[99]. According to their TPD and TOF experiments, after an initial adsorption in a bidentate configuration, acetaldehyde can give rise to either formate species by ejection of a methyl radical into the gas-phase or acetate via transferring the α-hydrogen to a bridging-oxygen site. Hauchecorne *et al.*[29] proposed instead different degradation mechanisms for molecularly adsorbed acetaldehyde and crotonaldehyde (Fig.13), the latter derived from aldol condensation of adsorbed acetaldehyde (see Section 2.1.2).

On the grounds of the proposed mechanisms, the reactive species involved in acetaldehyde photocatalytic degradation are likely photogenerated charges, in particular holes, h^+[36,120], as also supported by charge carrier lifetimes determined by time-resolved studies[121]. However, there are few reports suggesting a main role of $OH^{\bullet}$ radicals[122,123], especially in the presence of water

vapor, as these species are formed by the oxidation of hydroxyls and water molecules adsorbed by the photo-formed holes.

3.1.3 Acetic acid

Starting from the seminal works by Kraeutler and Bard[124], the photocatalytic degradation of acetic acid in water by TiO_2 has been extensively investigated in the literature[102,124,125]. On the other hand, the gas-phase reaction has received far less attention[94].

The main reaction intermediates of acetic acid photocatalytic degradation in the presence of oxygen and water include methanol, acetone, methane, methyl acetate[89] and methyl formate[91]. Experiments with isotopic markers show that the CH_3 group of acetic acid remains unchanged in the intermediates[89], ruling out degradation mechanisms based on the H-abstraction from the methyl group by $^{\bullet}OH$ radicals. There is the substantial agreement that the first step of the reaction on non-platinized TiO_2 is a direct oxidation of acetic acid by holes[89,94]. Indeed, acetate is a more efficient hole acceptor than methanol[126]. The hole-mediated process leads to decarboxylation through the cleavage of the C-C bond via photo-Kolbe reaction[124,127]. Hence, the decarboxylation step produces CO_2 and methyl radicals, as proved by ESR experiments[102]; the latter can react with surface OH or H, as well as give radical coupling reactions, leading to the described intermediates[89] (Fig.14). Indeed, during the photocatalytic oxidation of $CH_3{}^{13}COOH$, while $^{13}CO_2$ production peaks shortly after exposure to UV irradiation, the rate of $^{12}CO_2$ production increases slowly[98]. Hence, the α-carbon oxidizes to CO_2 in a single step without the formation of long-lived intermediates, whereas the β-carbon forms CO_2 through methoxide, formaldehyde, and formate[90]. Methanol, which is the main intermediate of the initial photooxidation step[89], can give rise to formaldehyde by oxidation as well as to methyl formate and methyl acetate[94]. Also acetaldehyde and acetone are probably resulting from methanol[89] and they are not obtained from reduction of the acetic acid -COOH moiety, as shown by Ngo *et al.* who observed non-marked acetone and acetaldehyde molecules during experiments with marked acetic acid ($CH_3{}^{13}COOH$)[94].

3.2 Effect of oxygen

Studies on single-crystal TiO_2 showed that background O_2 is required for ethanol photocatalytic oxidation[39,55,56]. Irradiation of anatase(101) in the absence of O_2 gives rise to small amounts of gas-phase photoreaction products (H_2, CH_3CHO, and $CH_3^{\bullet}$)[55], in line with reports on rutile(110) surfaces[39,56]. The acetaldehyde amount detected in the gas-phase increased with increasing doses of O_2[55,56,83,88], suggesting that the O_2 main role in this first stage is acceptor of photogenerated

electrons, which decreases the electron−hole recombination rate. This conclusion is supported also by FTIR results: Guzman *et al.*[30] compared the intensity of the background shift, measured as the IR absorbance intensity at 2000 cm^{-1}, while pulsing O_2 over ethanol adsorbed on TiO_2 (Fig.15). They observed a decrease in the background shift intensity indicated that O_2 directly reacted with photogenerated electrons ($O_{2ad} + e^- \rightarrow O_2^-$). Walenta *et al.*[88] reported the surface accumulation of acetaldehyde upon photoxidation on reduced rutile(110) in the absence of O_2 at low temperature (110 K); saturation was reached at 15% with respect to ethanol. Hansen *et al.*[26] detected acetaldehyde formation upon UV irradiation in UHV conditions for both reduced, oxidized and hydrogenated rutile(110) surfaces, although also in this case a fast saturation was observed. Both authors discuss this result in terms of upward band bending in the semiconductor, which can cause a preferential movement of photogenerated holes to the surface defects, while photogenerated electrons travel into the bulk.

Nadeem *et al.*[56] reported a 0.5 reaction order of O_2 partial pressure at near saturation coverage of ethanol/ethoxide on rutile(110) surfaces, suggesting that two O_2 molecules are required for the formation of an acetaldehyde molecule, which is a two-electron/hole-transfer reaction. A lower reaction order (0.15) for the ethanol to acetaldehyde conversion was reported by Katsiev and coauthors[55] on anatase(101), which they attributed to the weak equilibrium O_2 binding constant on the TiO_2 surface, which requires to increase the oxygen pressure for reaction.

Oxygen radicals are thought to participate directly in the formation of carboxylates from acetaldehyde species[30,39,55,56]. Pump-probe measurements over rutile(110) showed that the emission of $CH_3^{\bullet}$ radicals upon UV irradiation takes place only in the presence of O_2 (either in the atmosphere or preadsorbed)[83], indicating its participation in the acetaldehyde oxidation step leading to methyl radicals and adsorbed carboxylates. It is noteworthy that a shift in product selectivity from acetaldehyde (obtained by dehydrogenation reactions) to methyl radicals (produced by C-C cleavage pathways) was reported at increasing O_2 pressure in the case of ethanol photocatalysis over rutile(110) surfaces[55]. On the other hand, studies on anatase(101) surfaces showed a negligible C-C bond dissociation pathway at all investigated O_2 pressures[55].

The crucial role of oxygen has been related also to self-inhibiting effects[128]. Self-inhibition in the rate of ethanol photodecomposition was reported[88,129] and attributed to a site-blocking effect by the pre-adsorbed ethanol (or reaction intermediates) inhibiting the interaction between molecular oxygen and surface defects on TiO_2 surfaces[30,40]: the sticking probability of O_2 on a fully oxidized TiO_2 surface is negligible[130] and even on defective TiO_2, being many orders of magnitudes lower than the sticking coefficient of ethanol[57]. Indeed, the adsorption of O_2 at the TiO_2 surface was reported as the rate determining step in ethanol photocatalytic degradation[30].

Most of the reported studies about acetaldehyde degradation involve O_2 and oxidized TiO_2 surfaces. However, there are few conflicting reports about photocatalysis of acetaldehyde in the absence of O_2. Several authors[36,120] reported that no acetaldehyde photochemistry could take place on a reduced TiO_2(110) surfaces without the presence of adsorbed oxygen. Conversely, Xu and coworkers reported acetaldehyde degradation on reduced TiO_2(110) surfaces in the absence of O_2[99]. Such a difference was attributed by the authors to the different light source used during photoactivity tests, much more powerful (pulsed laser) in work of Xu and coauthors, and to differences in the electron impact ionization detection. This comparison points out that the photodissociation cross-section of acetaldehyde on rutile(110) is much smaller in the absence of oxygen. Xu *et al.*[99] proposed two reaction channels for the photocatalytic degradation of acetaldehyde in the absence of O_2, both involving surface oxygen species to produce acetate and formate species. As formate and acetate were detected also in experiments carried out without pre-oxidation of the photocatalyst surface, a bridge-bonded oxygen is likely the source of the required additional oxygen atom[99] via the formation of a bidentate acetaldehyde intermediate.

In the case of acetic acid, it is instead well accepted that the reaction can proceed even without molecular oxygen. However, although the photocatalytic degradation of acetic acid can take place also in the absence of oxygen[94], the presence of O_2 largely increases the reaction rate[81,98] (Tab.1), as it extends the hole lifetime by capturing photogenerated electrons[91]. Tab.1 also suggests that acetic acid has a slower degradation kinetics than that of ethanol, supporting earlier reports of a lower photocatalytic activity of TiO_2 toward carboxylates with respect to alcohols[57,81,131]. The absence of O_2 was reported to increase the amount of adsorbed acetic acid relatively to experiments in air[94], possibly due to a change in the adsorption mode. Most importantly, the detected reaction intermediates vary depending on the presence of O_2[91,94,98]. While decarboxylation is the first step under both atmospheres, the observed differences arise from the fate of the methyl group. In an oxygen-containing atmosphere, both carbon atoms of acetic acid can be transformed into CO_2[98], leading to a complete mineralization.

On the contrary, in an oxygen-free atmosphere, a complete mineralization is never achieved[98] as only the COOH group (α-carbon) is transformed into CO_2[90], while the β-carbon gives rise to alkanes, such as methane and ethane[94]. Without O_2 acting as photogenerated electron-acceptor, CH_4 is always detected and its formation is generally attributed to $H^{\bullet}$ radicals formed from the reduction of adsorbed H^+ from acetic acid by photogenerated electrons[94,132]. Specifically, there are conflicting reports about the formation of methane and ethane in the presence of oxygen[89,94,98]. Zhang *et al.* reported the appearance of methane after acetic acid was completely oxidized, suggesting that it was produced from the reaction of methanol and acetone[89]. Ngo *et*

al.[94] reported the formation of ethane at high coverage, supporting its formation via the combination of two methyl radicals; they suggested that ethane formation can occur via the reaction of a methyl radical with an irreversibly adsorbed acetic acid molecule.

3.3 Effect of water

Comparatively few studies have considered the role of water vapor on the photocatalytic degradation pathway. This is partly due to the aforementioned experimental difficulties in studying hydrated surfaces. As a result, photocatalytic degradation mechanisms at high relative humidity (RH) still remain highly speculative[16].

Water vapor depresses largely the photocatalytic oxidation of ethanol, due to the competition of water molecules for the photocatalyst surface sites[43,115], which hinders the interaction of ethanol with the surface[95,123].

In the case of acetaldehyde, there are mixed reports about the role of water vapor on the photocatalytic degradation rate, with some authors describing a marked detrimental effect of humidity on molecule disappearance[95,133] and others reporting enhanced mineralization in the presence of water vapor[123,133] (Fig.16). The slower kinetics of acetaldehyde disappearance on pristine TiO_2 was related to its decreased adsorption in humid conditions, due to competition with water molecules[34,95,134]. Conversely, the increase mineralization was attributed by Takeuchi *et al.*[123] to a faster degradation by $^{\bullet}OH$ radicals formed by the photo-oxidation of adsorbed water molecules. As the role of $^{\bullet}OH$ radicals in acetaldehyde degradation is still debated, an alternative explanation based on the change in adsorption mode, favoring reversible adsorption in humid conditions, can be hypothesized in analogy with acetic acid results (see also Section 4).

On the other hand, there is substantial agreement that the photocatalytic degradation of acetic acid is faster in the presence of water[123,129,135]. Several explanations have been put forward[89,123]. A possible role of the different adsorption modes of acetic acid with and without surface water was hypothesized[89]. Indeed, kinetic isotope studies and PDOS calculations supported a degradation originating from direct oxidation by holes, rather than from $^{\bullet}OH$ radical attack, even in humid conditions[89]. PDOS calculations of different adsorption modes of acetic acid revealed that the coordination geometry favored in the presence of water (monodentate acetic acid) is more easily oxidized by holes than the bidentate coordination; indeed, the former retains a higher electron density on the O 2p atom upon coordination with the surface Ti site, which is essential to favor hole transfer to this O atom[89].

4. Role of the photocatalyst features

4.1 TiO_2-based materials

The photocatalytic oxidation of ethanol, acetaldehyde and, to a lesser extent, acetic acid has been widely used as benchmark for comparing the photocatalytic activity of different systems. Extensive research efforts have been devoted to the evaluation of the photocatalytic performance of both commercially available photocatalysts and laboratory-made ones. Besides single crystals, commercial powders are mostly investigated in mechanistic and kinetics studies. Among them, Evonik P25 is up to now the most investigated photocatalyst thanks to its availability, cheapness and good photocatalytic performance[30,32,85,90,91,94,95,114]. Micrometric commercial TiO_2 powders has been recently proposed as an alternative to nanometric materials[136]. Besides powders, films[18,137,138], porous and other supported materials[139–143] have been tested. Moreover, a broad range of modifications of TiO_2 have been investigated for the degradation of our target pollutants, including metallization[102,144–147], doping[27,104,107,148], coupling with other semiconductors[149,150] or with high surface area materials[151], fluorination[42,97,152] and sulfonation[63,152]. Thermal treatments to improve the sample crystallinity are often reported, mainly calcination[18,107,123,145,148–150] and hydro/solvothermal procedures[147,151,153]. The post-synthetic treatment affects two key photocatalyst parameters for air remediation: surface area and surface hydroxylation[154].

Tab.2 reports an overview of some key characteristics of selected TiO_2-based materials used for ethanol, acetaldehyde, and acetic acid photocatalytic degradation, highlighting the relevant synthetic details.

Recently, the effect of noble metal deposition (Pt, Au, Ag) on the adsorption and degradation mechanism of ethanol[31,35,145,146,155–158], acetaldehyde[147] and acetic acid[102,144] has received increasing attention. Gold and platinum nanoparticles have been shown to play a key role in the selective ethanol adsorption providing sites for hydrogen abstraction from adsorbed surface ethoxy species, therefore resulting in the formation of acetaldehyde, linearly bonded to Ti^{4+} sites, and H_2[31,146,157]. Hence, noble metals do promote ethanol oxidation to AcH[146,156], but mixed results were reported on acetaldehyde further oxidation[156,159]. Tan et al.[31] proposed that the so-generated acetate species can go through further oxidation reactions to form oxalate, thanks to the synergistic effect between gold and TiO_2. The oxalate species can in turn undergo the C−C cleavage on the acidic surface sites of titania, thus forming formate species, which is finally converted to CO and CO_2 molecules through further dehydration and oxidation steps. Furthermore, additional reaction intermediates have been reported for ethanol oxidation over noble-metal-modified TiO_2, such as ethylene[157], butene[156] and oxalate[31] (Fig.17).

The effect of sulfate-modification on the adsorption and reactivity of acetaldehyde[63] and ethanol[145] at the TiO_2 surface was also reported. Aldehyde condensation reactions, giving rise to undesired species with higher molecular mass, can be suppressed by addition of noble metals[32], or via modification with sulfates[63]. In particular, crotonaldehyde formation in sulfate modified TiO_2 is hindered due to interactions between the carbonyl group of adsorbed acetaldehyde and the electron-rich sulfate: this stabilizing bond prevents further nucleophilic attacks, thus hindering aldol condensation[63]. This change in adsorption properties has important consequences in terms of reaction rate and on the photocatalyst reusability (see Section 5).

The role of surface fluorination on acetaldehyde adsorption and reactivity was investigated[42,97]. Kim *et al.* reported that surface fluorination markedly decreases, up to 30%, the amount of adsorbed acetaldehyde[97]. Surface fluorination of TiO_2 is known to inhibit the adsorption of molecules forming attractive interactions with surface hydroxyl groups. As TiO_2 surface can be expected to be fully hydroxylated/hydrated in their experimental conditions[97], a preferential reversible molecular adsorption can be hypothesized, explaining the marked influence of surface fluorination. The occurrence of aldol condensation upon acetaldehyde adsorption was also reported in fluorinated TiO_2[42]. Despite the loss in acetaldehyde adsorption, fluorination promoted the photocatalytic oxidation of acetaldehyde on TiO_2[97].

4.2 Other photocatalysts

While being the archetypal photocatalytic semiconductor, the large band gap energy of TiO_2, suitable only for UV-light activation, the fast charge carriers recombination together with the emerging health concerns hinder its large-scale application. In the last decades, other photocatalysts have been proposed as efficient alternatives, including WO_3[160,161], graphitic carbon nitride (g-C_3N_4[162–164]), $SrTiO_3$[165], Bi_2O_3[166,167] and metal-organic frameworks (MOFs)[168,169].

Concerning especially acetaldehyde photodegradation, many endeavors have been made up to now and in particular in the very recent decades. A thorough outlook on the latest photocatalysts exploited to photodegrade acetaldehyde is reported in Table 3. Most of them have been engineered to be potentially used under simulated solar/visible light. Specifically, several authors focused their efforts towards the development of photocatalysts based on differently modified polymeric graphitic carbon nitride (g-C_3N_4) materials, thanks to their low cost, unique chemical stability, environmental friendliness and tunable microstructure[164] (see Table 3). Promising results were achieved by coupling metal oxide nanoparticles (like SnO_2[164] and WO_3[162]) to g-C_3N_4 aiming to form nano-heterojunctions able to slow down the charge carrier recombination, concomitantly boosting the final photocatalytic efficiency.

Besides, another emerging material that can enhance the light harvesting is mica: by introducing this compound into metal oxide networks, thus forming ternary systems[170], an augmented photocatalytic response can be obtained thanks to the insertion of reflection centers[171]. Indeed, the transmitted light that reaches mica can be reflected to the metal oxide being harvested and utilized, so that much more e^- and h^+ pairs are photoinduced. For instance, in a system composed by mica/TiO_2/rGO[171], hydroxyl radicals are generated by the interaction between holes and water, leading to the decomposition of pre-adsorbed acetaldehyde through a step-pathway comprising the possible formation of acetic acid, formaldehyde, formic acid and finally CO_2.

Furthermore, a very novel work by Gao *et al.*[168] has shown that the N,Zn co-doping of metal organic frameworks (MOFs, namely MIL-125(N-Ti_9Zn_1)) surface can provide a synergistic effect, efficiently degrading gaseous aldehyde molecules under humid conditions (relative humidity of 80%). Indeed, MOFs are believed to be promising photocatalysts (having huge surface area, tunable surface modification, high density and dispersion of active metal sites) even if some significant drawbacks should be overcome, such as the low photosensitivity. Gao *et al.*[168] observed enhanced performances due to the N,Zn co-doping that can augment the ability of activating oxygen and H_2O molecules into superoxide ($O_2^{-\bullet}$) and hydroxy radicals ($OH^\bullet$), showing a ten-fold faster reaction kinetics with respect to the pristine metal organic framework. Actually, the proposed reaction mechanism, triggered by visible light, contemplates the electrons excitation to the conduction band of MOF ligands, leaving the holes at the valence band of MOF. In this process, the dopants (Zn and N) act as a shallow trap, efficiently avoiding the recombination of electron-hole pairs. Vaporous acetaldehyde is firstly adsorbed and enriched on the surface of MIL-125(N-Ti_9Zn_1), and then reacts with positive holes or generated radicals oxidizing into CH_3COOH intermediate and finally CO_2 and H_2O.

To sum up, the newly designed photocatalysts herein reported can give an idea of the current investigated materials exhibiting promising features for the photocatalytic abatement of several VOCs, as already shown in the case of acetaldehyde model molecules.

5. Photocatalyst deactivation

Photocatalyst deactivation due to site-blocking by strongly bonded intermediate products can severely deteriorate the photocatalyst efficiency and lifetime. This issue is particularly relevant in gas-phase photocatalysis, where there is no water solvent to help to remove products and intermediates from the surface[17]. Deactivation occurs even upon the gas-phase photocatalytic degradation of relatively small molecules, such as ethanol and acetaldehyde, after a limited number of recycle tests with pollutant concentrations in the ppm range[63,88,95,152,172].

The loss of photocatalytic activity has been related to changes in adsorption properties of the photocatalyst surface. In the case of ethanol, dark adsorption on fresh TiO_2 follows a Langmuir isotherm, whereas upon consecutive photocatalytic degradation experiments a non-Langmuirian behavior was reported and related to the formation of organic deposits[95]. Such effects do not seem related to carbon deposits, as no coking was observed upon photocatalytic degradation of ethanol by Auger spectra[88]. Topalian *et al.*[63] reported an accumulation of carboxylate species (in particular formate) upon consecutive photocatalytic tests of acetaldehyde over TiO_2. Also Guzman and coauthors[30] reported a detrimental effect of acetate species stably adsorbed at the TiO_2 surface on the photocatalytic degradation of ethanol, blocking the O_2 access to the surface[106].

Water is a byproduct of photocatalytic oxidation of our model pollutants and its accumulation during photocatalytic tests is thus unavoidable[88]. As discussed in Section 3.3, water vapor can have beneficial effects, as for the photocatalytic degradation of acetic acid[127], but it can also compete for adsorption with ethanol and acetaldehyde[88,96], decreasing their degradation rate[95,123]. During ethanol photocatalytic degradation on rutile(101), Walenta *et al.*[88] reported a site-blocking effect of oxygen vacancies by water molecules, on the grounds of the absence of O_2 photon-stimulated desorption upon O_2 dosing after thermal removal of adsorbed ethanol and acetaldehyde molecules. They restored the surface activity upon heating at temperatures >450 K, which was attributed to the removal of adsorbed water molecules.

Piera *et al.*[95] investigated several surface treatments aimed at restoring the photocatalytic activity of used TiO_2. The tested regeneration procedures involved prolonged treatment under dry or humid air flux at temperatures up to 150 °C and treatments with vaporized H_2O_2 solutions. The combination of clean air and irradiation has also been tested to restore the activity of TiO_2 upon ethanol degradation tests[173]. However, none of these treatments proved able to completely recover the TiO_2 initial dark adsorption properties nor the photocatalytic activity. In particular, treatment at 80-150 °C can be counterproductive as it can favor the transformation of some of the surface-bound intermediates to less volatile species[95]. Treatments with H_2O_2 or UV seemed to be more effective, even though a complete recovery of the photocatalyst properties was never achieved[95,173]. As mentioned above, higher temperatures (above 450 K) can be used to thermally remove adsorbed species and to re-oxidize to surface from the bulk, thus replenishing the surface defects acting as adsorption sites[88].

Besides using regeneration treatments, the lifetime of a photocatalyst can be prolonged by engineering its properties. Antonello *et al.*[18] reported mechanically stable TiO_2 films showing

limited loss in photocatalytic activity upon recycle tests, without any regeneration treatment, with respect to P25 Evonik films.

The modification of the photocatalyst surface acidity was proposed as a suitable strategy to enhance byproduct desorption and promote the photocatalyst reusability[63]. Desorption is generally a rate-determining step in photocatalysis, and it depends on the acid-base properties of the photocatalyst surface. The modification of TiO_2 surface with sulfate groups weakens the adsorption of aldehyde and carboxylate species and, in particular, it prevents the formation of crotonaldehyde via aldol condensation[63]. Different reaction pathways have been proposed for the photocatalytic oxidation of crotonaldehyde and adsorbed acetaldehyde[29], the rate-determining step of the former being formate photo-oxidation (and CO_2 desorption), and acetaldehyde photo-oxidation for the latter. Hence, upon sulfate-modification, the formation rate of formate species lowers and becomes smaller than formate desorption or conversion to other intermediates: this prevents the accumulation of site-blocking formate intermediates and promotes acetaldehyde adsorption capacity in repeated tests and a higher sustained reactivity of the photocatalysts[63].

The modification of TiO_2 with selected metals (Pd, Cu) has also proven a promising strategy to reduce deactivation phenomena[152]. Arana and coworkers[152] attributed deactivation phenomena observed after repeated photocatalytic degradation tests of ethanol on pristine TiO_2 and Fe-modified TiO_2 to the surface accumulation of acetate species. The formation of acetates was attributed to the reaction of ethoxides, created by ethanol adsorption on photocatalyst surfaces rich in H-bonded hydroxyls, and $O_2^{-\bullet}$ radicals, generated by reduction of adsorbed O_2 by photo-promoted electrons. Titania modification with Pd and Cu lowers the content in H-bonded hydroxyls, promoting different adsorption modes of ethanol molecules at the photocatalyst surface; moreover, Pd and Cu oxides can capture photogenerated electrons, thus slowing down the formation of $O_2^{\bullet-}$ radicals linked to acetate generation.

6. Modeling realistic indoor conditions

Most literature studies report photocatalytic tests in unrealistic conditions: batch tests, often in dry air and without other pollutant species competing with the main target molecule. Conversely, the successful application of photocatalytic technologies to the removal of VOCs in air purifiers requires a better understanding of the role of operational and environmental parameters in continuous reactors.

Air purifier technologies (both stand-alone air cleaners and units integrated into heating, ventilation and air conditioning, HVAC, systems) work in continuous mode with airflow velocities that can reach several hundreds of cubic meters per hour[174]. As in gas-phase photocatalysis only the

adsorbed molecules can undergo redox reactions by photogenerated charge carriers or surface radicals, therefore mass transfer and contact time are key parameters. While in batch reactors, commonly used at lab-scale, contact times range from seconds to minutes, continuous set-ups employ high airflow rates to maximize mass transfer but, in doing so, very short contact times between the pollutant and the photocatalyst surface (in the order of seconds or less) are obtained[175]. Sub-optimal contact times between the pollutant and the active surface can result in incomplete degradation of the pollutant and potential accumulation of undesired, toxic byproducts[14,176]. Aldehydes, such as acetaldehyde, feature among the most common toxic degradation intermediates, prone to accumulation especially in the presence of pollutant mixtures[176,177]. As a result, Héquet *et al.* proposed to monitor acetaldehyde and formaldehyde for the evaluation of the efficiency of photocatalytic air purifiers for indoor applications[177].

Reactor design and operating parameters are pivotal in ensuring the effective removal of primary pollutants and minimizing the formation of secondary byproducts. Destaillats *et al.*[174] studied the degradation of a mixture of pollutants including acetaldehyde, by a prototype air cleaner operating in recirculation mode at flow rates in the range 178–878 $m^3\ h^{-1}$. They found that the removal efficiency for highly volatile species, such as formaldehyde and acetaldehyde, improved significantly using longer contact times: it is noteworthy that a net production of formaldehyde was observed at high flow rates, while net removal was determined when longer contact times were ensured (Fig.18). They also reported that using pleated, instead of flat, support increased the performance by extending the dwelling time of pollutants on the irradiated photocatalyst surface.

Zhong and Haghighat[14] investigated the role of several operational (airflow rate, light intensity) and environmental (ethanol concentration, RH, ozone concentration) parameters on byproduct concentrations (formaldehyde and acetaldehyde) of ethanol photocatalytic degradation by TiO_2–coated fiberglass filters in a pilot duct reactor operating in open-loop mode with airflow up to 270 $m^3\ h^{-1}$ under UV irradiation (Fig.19). They found a positive correlation between inlet ethanol concentration and acetaldehyde concentration, but not with formaldehyde, which is indicative of poor mineralization (Fig.19a). Higher pollutant concentrations are generally associated with improved reaction rates, but also with poorer removal efficiency and lower mineralization[178]. The observed trend in terms of airflow rate suggests that surface photochemical reaction rate, rather than the mass transfer between gas and solid phases, was the controlling step in the adopted conditions (Fig.19b). Higher relative humidity promoted mineralization, although a complete ethanol disappearance was not achieved (Fig.19c), while higher irradiance heightened byproduct concentration as it increased ethanol oxidation rate (Fig.19d). The addition of ozone did not affect

acetaldehyde and formaldehyde formation, but gave rise to trace amounts of other byproducts, such as acetone, crotonaldehyde, and propionaldehyde[14].

Few attempts of modeling the photocatalytic degradation of ethanol and acetaldehyde have been reported in the literature[140,179]. As photocatalytic reactor performance depends on numerous parameters (light distribution, mass transfer via convection and diffusion, air flow, photocatalytic reactions), multiphysics models combining light distribution models, air flow dynamics models, and photocatalytic reaction kinetic models[180] are needed to better design, upscale, and optimize these reactors. For instance, van Walsem *et al*.[181] applied computational fluid dynamics (CFD) to model acetaldehyde degradation in a multi-tube reactor under UV irradiation with an incident intensity of 2.1 mW cm^{-2} (Fig.20a). CFD modeling enabled them to consider the whole reactor geometry and flow parameters, leading to a model that could accurately simulate simultaneous adsorption, desorption and photocatalytic degradation (Fig.20b).

Models should be validated using realistic conditions, possibly relying on standardized tests. Weon *et al*.[13] equipped a commercial air-cleaner (Samsung, AX7000) with two 273×308 mm^2 TiO_2 nanotube filters and 30 UV-LEDs and tested its VOCs removal efficiency according to the Korean air cleaner standards protocol SPS-KACA002-132 (Fig.21). Tests were carried out in a 8 m^3-test chamber at 23 °C and RH=55%, towards the removal of various VOCs, including acetaldehyde and acetic acid, each at 10 ppmv initial concentration. An average VOCs removal efficiency of 72% was obtained in 30 min of operation (95.2% and 58.7% for acetic acid and acetaldehyde, respectively). This system was the first photocatalytic air cleaner to pass the SPS-KACA002-132 protocol.

Other studies[9,181] have reported acetaldehyde photocatalytic degradation tests based on the ISO 22197-2:2011 standard[182], which adopts a 5 ppmv acetaldehyde concentration, a 1.0 dm^3 min^{-1} air flow, RH=50%, 1.0 mW cm^{-2} UV-A irradiation and 3 h test time[183]. The ISO 22197-2:2011 standard has been revised by ISO 22197-2:2019 standard test method for air-purification performance towards acetaldehyde of photocatalytic ceramics and structured filter materials.

van Walsem *et al*.[181] adopted a multi-tube reactor for the photocatalytic oxidation of acetaldehyde under HVAC operating conditions (flow velocity 2–2.5 m s^{-1}, 5 ppmv, RH=50%, UV-A, 10 h duration) in an airtight climate chamber build according to the French standard AFNOR XP B44–013[184] reporting a mass-transfer limited kinetics. Costamarrone and coauthors compared commercial photocatalytic air purifiers in standardized chamber tests in accordance with the AFNOR XP B44–013 standard[185,186] and its replacement, the European standard NF EN 16846-1:2017[187]. The device performance towards the abatement of a mixture of VOCs including acetaldehyde were evaluated in terms of Clean Air Delivery Rate (CADR), secondary product

emission and mineralization rate. They also reported pilot experiments in 35–40 m^3 rooms using VOC emitted by furniture[186] and evaluated nanoparticles release from the photocatalytic material[185].

7. Conclusions and outlook

This review has outlined the current understanding on the adsorption and photocatalytic oxidation mechanisms of three selected model VOCs, *i.e.* ethanol, acetaldehyde and acetic acid. Notwithstanding the important differences among the three pollutants, some general conclusions can be drawn.

Most literature studies are focused on dehydroxylated/dehydrated surfaces. On this kind of surfaces, dissociative adsorption has been reported for ethanol and acetic acid, and reactive adsorption has been reported for acetaldehyde, leading to the formation of adsorbed crotonaldehyde. For each pollutant, adsorption involves the formation of interactions between the oxygen atoms of the organic molecules with surface Ti_{5c} centers, favoring adsorption on oxygen defect sites for ethanol and acetaldehyde. Notably, the presence of water molecules affects the adsorption of the three pollutants both in terms of adsorption competition, especially for ethanol and acetaldehyde, and by modifying the adsorption geometry in favor of monodentate and molecularly adsorbed species.

Light irradiation elicits the photocatalytic oxidation of the three molecules, which can proceed to partial or complete mineralization. Most of the literature identified reaction pathways driven by photogenerated holes. However, depending on the surface coverage and presence of water molecules, the occurrence of hydroxyl radicals mediated pathways has been reported, in particular for ethanol and acetaldehyde. On the other hand, molecular oxygen plays an essential role as electron acceptor, increasing the reaction rate, and its presence is essential to achieve a complete mineralization, also for acetic acid. Mechanisms involving a direct attack of oxygen radicals have been proposed for ethanol and acetaldehyde. The conclusions drawn from these simple model molecules could be used to predict the adsorption and photocatalytic behavior of analogues with higher number of carbon atoms[188].

However, numerous gaps in our knowledge remain unsolved. While adsorption on fresh and dehydrated TiO_2 surfaces is relatively known, the interaction of our model VOCs with real photocatalyst surfaces is far less understood. Water molecules play a complex and crucial role on all the steps of the photocatalytic process, from adsorption to reaction mechanism, from kinetics to photocatalyst reusability. Their presence is unavoidable in real systems, partly because water is among the final oxidation products. However, the role of water on the adsorption and photocatalytic oxidation of ethanol, acetaldehyde and acetic acid is still debated in the literature, as several

experimental techniques cannot be applied to fully hydrates surfaces and theoretical approaches often do not involve water molecules due to computational costs. Moreover, further research should shed light on the interfering effects of other common air pollutants, both in terms of competition for adsorption at the photocatalyst surface and of reaction pathways.

Another topic that deserves further study is the deactivation mechanism of photocatalysts and possible strategies to restore their activity. The occurrence of photocatalyst deactivation has been consistently reported even for the gas-phase degradation of small molecules such as ethanol and acetaldehyde; particularly, it has been related to strongly bound intermediates (carboxylates) or products (water molecules), thus blocking the photocatalyst surface sites. A promising strategy to tackle this problem is the surface modification: increasing the photocatalyst surface acidity (*e.g.,* with sulfate groups) has been reported to slow down deactivation phenomena.

While a broad range of photocatalysts have been tested towards the degradation of ethanol and acetaldehyde and, to a lesser extent, of acetic acid, they are mostly based on TiO_2 materials. The photocatalyst surface features (*i.e.* specific area and acidity) have been reported to play a crucial role in the overall reaction kinetics and stability to deactivation. Recently, other semiconductors have been proposed as visible-light alternatives to TiO_2 systems, including g-C_3N_4, WO_3 and MOFs, but adsorption mechanisms and reaction pathways for these emerging photocatalysts remain to be deeply unravel.

Comparatively, few reports presented tests in continuous reactors adopting realistic conditions in terms of airflow, irradiance, pollutant concentration, relative humidity and other interferents. These studies consistently showed that, when sub-optimal conditions are adopted, the photocatalytic oxidation can lead to accumulation of acetaldehyde and other highly volatile byproducts. Because of its potential for accumulation, acetaldehyde has so far received the most attention in terms of standard tests for photocatalytic reactors. In this respect, modeling studies can offer valuable predictive tools to simulate adsorption and photocatalytic oxidation in complex reactor geometries, thus guiding the design and dimensioning of better performing configurations.

An in-depth understanding of the adsorption and photodegradation mechanisms of ethanol, acetaldehyde and acetic acid would thus have far reaching consequences in terms of innovation potential. By highlighting the current state of the art and open challenges, this review aims at stimulating further research on this topic.

Funding details. This research did not receive any specific grant from funding agencies in the public, commercial, or not-for-profit sectors.

Disclosure statement. The authors have no conflict of interest to declare.

Data availability statement. Not applicable.

References

1. WHO *Economic cost of the health impact of air pollution in Europe*; **2015**.
2. Brasche, S.; Bischof, W. Daily time spent indoors in German homes – Baseline data for the assessment of indoor exposure of German occupants. *Int. J. Hyg. Environ. Health* **2005**, *208*, 247–253.
3. Hwang, H.-M.; Park, E.-K.; Young, T.M.; Hammock, B.D. Occurrence of endocrine-disrupting chemicals in indoor dust. *Sci. Total Environ.* **2008**, *404*, 26–35.
4. Weschler, C.J.; Nazaroff, W.W. Semivolatile organic compounds in indoor environments. *Atmos. Environ.* **2008**, *42*, 9018–9040.
5. Weschler, C.J. Changes in indoor pollutants since the 1950s. *Atmos. Environ.* **2009**, *43*, 153–169.
6. Net, S.; Sempéré, R.; Delmont, A.; Paluselli, A.; Ouddane, B. Occurrence, Fate, Behavior and Ecotoxicological State of Phthalates in Different Environmental Matrices. *Environ. Sci. Technol.* **2015**, *49*, 4019–4035.
7. Baez, A.; Padilla, H.; Garcia, R.; Torres, M.; Rosas, I.; Belmont, R. Carbonyl levels in indoor and outdoor air in Mexico City and Xalapa, Mexico. *Sci. Total Environ.* **2003**, *302*, 211–226.
8. Salvadores, F.; Minen, R.I.; Carballada, J.; Alfano, O.M.; Ballari, M.M. Kinetic Study of Acetaldehyde Degradation Applying Visible Light Photocatalysis. *Chem. Eng. Technol.* **2016**, *39*, 166–174.
9. Krýsa, J.; Baudys, M.; Vislocka, X.; Neumann-Spallart, M. Composite photocatalysts based on TiO_2 – Carbon for air pollutant removal: Aspects of adsorption. *Catal. Today* **2020**, *340*, 34–39.
10. Fujishima, A.; Zhang, X.; Tryk, D. TiO_2 photocatalysis and related surface phenomena. *Surf. Sci. Rep.* **2008**, *63*, 515–582.
11. Rimoldi, L.; Pargoletti, E.; Meroni, D.; Falletta, E.; Cerrato, G.; Turco, F.; Cappelletti, G. Concurrent role of metal (Sn, Zn) and N species in enhancing the photocatalytic activity of TiO_2 under solar light. *Catal. Today* **2018**, *313*, 40–46.
12. Cappelletti, G.; Pifferi, V.; Mostoni, S.; Falciola, L.; Di Bari, C.; Spadavecchia, F.; Meroni, D.; Davoli, E.; Ardizzone, S. Hazardous *o*-toluidine mineralization by photocatalytic bismuth doped ZnO slurries. *Chem. Commun.* **2015**, *51*, 10459–10462.
13. Weon, S.; Choi, E.; Kim, H.; Kim, J.Y.; Park, H.-J.; Kim, S.; Kim, W.; Choi, W. Active {001} Facet Exposed TiO_2 Nanotubes Photocatalyst Filter for Volatile Organic Compounds Removal: From Material Development to Commercial Indoor Air Cleaner Application. *Environ. Sci. Technol.* **2018**, *52*, 9330–9340.
14. Zhong, L.; Haghighat, F. Modeling of by-products from photocatalytic oxidation (PCO) indoor air purifiers: A case study of ethanol. *Build. Environ.* **2018**, *144*, 427–436.
15. Bianchi, C.L.; Cerrato, G.; Bresolin, B.M.; Djellabi, R.; Rtimi, S. Digitally Printed AgNPs Doped TiO_2 on Commercial Porcelain-Grès Tiles: Synergistic Effects and Continuous Photocatalytic Antibacterial Activity. *Surfaces* **2020**, *3*, 11–25.

16. Hauchecorne, B.; Lenaerts, S. Unravelling the mysteries of gas phase photocatalytic reaction pathways by studying the catalyst surface: A literature review of different Fourier transform infrared spectroscopic reaction cells used in the field. *J. Photochem. Photobiol. C Photochem. Rev.* **2013**, *14*, 72–85.

17. Paz, Y. Application of TiO_2 photocatalysis for air treatment: Patents' overview. *Appl. Catal. B Environ.* **2010**, *99*, 448–460.

18. Antonello, A.; Soliveri, G.; Meroni, D.; Cappelletti, G.; Ardizzone, S. Photocatalytic remediation of indoor pollution by transparent TiO_2 films. *Catal. Today* **2014**, *230*, 35–40.

19. Millet, D.B.; Apel, E.; Henze, D.K.; Hill, J.; Marshall, J.D.; Singh, H.B.; Tessum, C.W. Natural and Anthropogenic Ethanol Sources in North America and Potential Atmospheric Impacts of Ethanol Fuel Use. *Environ. Sci. Technol.* **2012**, *46*, 8484–8492.

20. Raillard, C.; Héquet, V.; Le Cloirec, P.; Legrand, J. Photocatalytic oxidation of methyl ethyl ketone over sol-gel and commercial TiO_2 for the improvement of indoor air. *Water Sci. Technol.* **2006**, *53*, 107–115.

21. Malayeri, M.; Lee, C.-S.; Haghighat, F. Modeling of photocatalytic oxidation reactor for methyl ethyl ketone removal from indoor environment: Systematic model development and validation. *Chem. Eng. J.* **2021**, *409*, 128265.

22. Bianchi, C.L.; Gatto, S.; Pirola, C.; Naldoni, A.; Di Michele, A.; Cerrato, G.; Crocellà, V.; Capucci, V. Photocatalytic degradation of acetone, acetaldehyde and toluene in gas-phase: Comparison between nano and micro-sized TiO_2. *Appl. Catal. B Environ.* **2014**, *146*, 123–130.

23. Debono, O.; Thevenet, F.; Gravejat, P.; Hequet, V.; Raillard, C.; Lecoq, L.; Locoge, N. Toluene photocatalytic oxidation at ppbv levels: Kinetic investigation and carbon balance determination. *Appl. Catal. B Environ.* **2011**, *106*, 600–608.

24. d'Hennezel, O.; Pichat, P.; Ollis, D.F. Benzene and toluene gas-phase photocatalytic degradation over H2O and HCL pretreated TiO_2: by-products and mechanisms. *J. Photochem. Photobiol. A Chem.* **1998**, *118*, 197–204.

25. Ding, X.; Liu, H.; Chen, J.; Wen, M.; Li, G.; An, T.; Zhao, H. In situ growth of well-aligned Ni-MOF nanosheets on nickel foam for enhanced photocatalytic degradation of typical volatile organic compounds. *Nanoscale* **2020**, *12*, 9462–9470.

26. Hansen, J.Ø.; Bebensee, R.; Martinez, U.; Porsgaard, S.; Lira, E.; Wei, Y.; Lammich, L.; Li, Z.; Idriss, H.; Besenbacher, F.; et al. Unravelling Site-Specific Photo-Reactions of Ethanol on Rutile TiO_2(110). *Sci. Rep.* **2016**, *6*, 21990.

27. Asahi, R.; Morikawa, T.; Ohwaki, T.; Taga, Y. Visible-Light Photocatalysis in Nitrogen-Doped Titanium Oxides. *Science* **2001,** *80*.

28. Stucchi, M.; Boffito, D.; Pargoletti, E.; Cerrato, G.; Bianchi, C.; Cappelletti, G. Nano-MnO2 Decoration of TiO_2 Microparticles to Promote Gaseous Ethanol Visible Photoremoval. *Nanomaterials* **2018**, *8*, 686.

29. Hauchecorne, B.; Terrens, D.; Verbruggen, S.; Martens, J.A.; Van Langenhove, H.; Demeestere, K.; Lenaerts, S. Elucidating the photocatalytic degradation pathway of acetaldehyde: An FTIR in situ study under atmospheric conditions. *Appl. Catal. B Environ.*

2011, *106*, 630–638.

30. Guzman, F.; Chuang, S.S.C. Tracing the Reaction Steps Involving Oxygen and IR Observable Species in Ethanol Photocatalytic Oxidation on TiO_2. *J. Am. Chem. Soc.* **2010**, *132*, 1502–1503.

31. Tan, T.H.; Scott, J.; Ng, Y.H.; Taylor, R.A.; Aguey-Zinsou, K.-F.; Amal, R. C–C Cleavage by Au/TiO_2 during Ethanol Oxidation: Understanding Bandgap Photoexcitation and Plasmonically Mediated Charge Transfer via Quantitative in Situ DRIFTS. *ACS Catal.* **2016**, *6*, 8021–8029.

32. Raskó, J.; Kiss, J. Adsorption and surface reactions of acetaldehyde on TiO_2, CeO_2 and Al_2O_3. *Appl. Catal. A Gen.* **2005**, *287*, 252–260.

33. Wang, C.; Groenzin, H.; Shultz, M.J. Comparative Study of Acetic Acid, Methanol, and Water Adsorbed on Anatase TiO_2 Probed by Sum Frequency Generation Spectroscopy. *J. Am. Chem. Soc.* **2005**, *127*, 9736–9744.

34. Batault, F.; Thevenet, F.; Hequet, V.; Rillard, C.; Le Coq, L.; Locoge, N. Acetaldehyde and acetic acid adsorption on TiO_2 under dry and humid conditions. *Chem. Eng. J.* **2015**, *264*, 197–210.

35. Bahruji, H.; Bowker, M.; Brookes, C.; Davies, P.R.; Wawata, I. The adsorption and reaction of alcohols on TiO_2 and Pd/TiO_2 catalysts. *Appl. Catal. A Gen.* **2013**, *454*, 66–73.

36. Zehr, R.T.; Henderson, M.A. Acetaldehyde photochemistry on TiO_2(110). *Surf. Sci.* **2008**, *602*, 2238–2249.

37. Pepin, P.A.; Diroll, B.T.; Choi, H.J.; Murray, C.B.; Vohs, J.M. Thermal and Photochemical Reactions of Methanol, Acetaldehyde, and Acetic Acid on Brookite TiO_2 Nanorods. *J. Phys. Chem. C* **2017**, *121*, 11488–11498.

38. Farfan-Arribas, E.; Madix, R.J. Role of Defects in the Adsorption of Aliphatic Alcohols on the TiO_2 (110) Surface. *J. Phys. Chem. B* **2002**, *106*, 10680–10692.

39. Jayaweera, P.M.; Quah, E.L.; Idriss, H. Photoreaction of Ethanol on TiO_2 (110) Single-Crystal Surface. *J. Phys. Chem. C* **2007**, *111*, 1764–1769.

40. Kim, Y.K.; Hwang, C.-C. Photoemission study on the adsorption of ethanol on clean and oxidized rutile TiO_2(110)-1×1 surfaces. *Surf. Sci.* **2011**, *605*, 2082–2086.

41. Ma, Z.; Guo, Q.; Mao, X.; Ren, Z.; Wang, X.; Xu, C.; Yang, W.; Dai, D.; Zhou, C.; Fan, H.; et al. Photocatalytic Dissociation of Ethanol on TiO_2(110) by Near-Band-Gap Excitation. *J. Phys. Chem. C* **2013**, *117*, 10336–10344.

42. Wang, Z.; Huang, J.; Amal, R.; Jiang, Y. Solid-state NMR study of photocatalytic oxidation of acetaldehyde over the flame-made F-TiO_2 catalyst. *Appl. Catal. B Environ.* **2018**, *223*, 16–21.

43. Pilkenton, S.; Hwang, S.-J.; Raftery, D. Ethanol Photocatalysis on TiO_2-Coated Optical Microfiber, Supported Monolayer, and Powdered Catalysts: An in Situ NMR Study. *J. Phys. Chem. B* **1999**, *103*, 11152–11160.

44. Muir, J.N.; Choi, Y.; Idriss, H. Computational study of ethanol adsorption and reaction over rutile TiO_2 (110) surfaces. *Phys. Chem. Chem. Phys.* **2012**, *14*, 11910.

45. Plata, J.J.; Collico, V.; Márquez, A.M.; Sanz, J.F. Understanding Acetaldehyde Thermal Chemistry on the TiO_2(110) Rutile Surface: From Adsorption to Reactivity. *J. Phys. Chem. C* **2011**, *115*, 2819–2825.

46. Yao, M.; Ji, Y.; Wang, H.; Ao, Z.; Li, G.; An, T. Adsorption Mechanisms of Typical Carbonyl-Containing Volatile Organic Compounds on Anatase TiO_2(001) Surface: A DFT Investigation. *J. Phys. Chem. C* **2017**, *121*, 13717–13722.

47. Manzhos, S.; Giorgi, G.; Yamashita, K. A Density Functional Tight Binding Study of Acetic Acid Adsorption on Crystalline and Amorphous Surfaces of Titania. *Molecules* **2015**, *20*, 3371–3388.

48. Hansen, J.Ø.; Huo, P.; Martinez, U.; Lira, E.; Wei, Y.Y.; Streber, R.; Lægsgaard, E.; Hammer, B.; Wendt, S.; Besenbacher, F. Direct Evidence for Ethanol Dissociation on Rutile TiO_2(110). *Phys. Rev. Lett.* **2011**, *107*, 136102.

49. Martinez, U.; Hansen, J.Ø.; Lira, E.; Kristoffersen, H.H.; Huo, P.; Bechstein, R.; Lægsgaard, E.; Besenbacher, F.; Hammer, B.; Wendt, S. Reduced Step Edges on Rutile TiO_2(110) as Competing Defects to Oxygen Vacancies on the Terraces and Reactive Sites for Ethano. *Phys. Rev. Lett.* **2012**, *109*, 155501.

50. Huo, P.; Hansen, J.Ø.; Martinez, U.; Lira, E.; Streber, R.; Wei, Y.; Lægsgaard, E.; Hammer, B.; Wendt, S.; Besenbacher, F. Ethanol Diffusion on Rutile TiO_2(110) Mediated by H Adatoms. *J. Phys. Chem. Lett.* **2012**, *3*, 283–288.

51. Tao, J.; Luttrell, T.; Bylsma, J.; Batzill, M. Adsorption of Acetic Acid on Rutile TiO_2(110) vs (011)-2 × 1 Surfaces. *J. Phys. Chem. C* **2011**, *115*, 3434–3442.

52. Gamble, L.; Jung, L.S.; Campbell, C.T. Decomposition and protonation of surface ethoxys on TiO_2(110). *Surf. Sci.* **1996**, *348*, 1–16.

53. Zhang, R.; Liu, Z.; Ling, L.; Wang, B. The effect of anatase TiO_2 surface structure on the behavior of ethanol adsorption and its initial dissociation step: A DFT study. *Appl. Surf. Sci.* **2015**, *353*, 150–157.

54. Kim, Y.K.; Kay, B.D.; White, J.M.; Dohnalek, Z. Alcohol Chemistry on Rutile TiO_2(110): The Influence of Alkyl Substituents on Reactivity and Selectivity. *J. Phys. Chem. C* **2007**, *111*, 18236–18242.

55. Katsiev, K.; Harrison, G.; Alghamdi, H.; Alsalik, Y.; Wilson, A.; Thornton, G.; Idriss, H. Mechanism of Ethanol Photooxidation on Single-Crystal Anatase TiO_2(101). *J. Phys. Chem. C* **2017**, *121*, 2940–2950.

56. Nadeem, A.M.; Muir, J.M.R.; Connelly, K.A.; Adamson, B.T.; Metson, B.J.; Idriss, H. Ethanol photo-oxidation on a rutile TiO_2(110) single crystal surface. *Phys. Chem. Chem. Phys.* **2011**, *13*, 7637.

57. Harrison, G.; Katsiev, K.; Alsalik, Y.; Thornton, G.; Idriss, H. Switch in photocatalytic reaction selectivity: The effect of oxygen partial pressure on carbon-carbon bond dissociation over hydroxylated TiO_2(110) surfaces. *J. Catal.* **2018**, *363*, 117–127.

58. Stefanov, B.I.; Topalian, Z.; Granqvist, C.G.; Österlund, L. Acetaldehyde adsorption and condensation on anatase TiO_2: Influence of acetaldehyde dimerization. *J. Mol. Catal. A Chem.* **2014**, *381*, 77–88.

59. Rekoske, J.E.; Barteau, M.A. Competition between Acetaldehyde and Crotonaldehyde during Adsorption and Reaction on Anatase and Rutile Titanium Dioxide. *Langmuir* **1999**, *15*, 2061–2070.

60. Lusvardi, V.; Barteau, M.A.; Farneth, W.E. The Effects of Bulk Titania Crystal Structure on the Adsorption and Reaction of Aliphatic Alcohols. *J. Catal.* **1995**, *153*, 41–53.

61. Singh, M.; Zhou, N.; Paul, D.K.; Klabunde, K.J. IR spectral evidence of aldol condensation: Acetaldehyde adsorption over TiO_2 surface. *J. Catal.* **2008**, *260*, 371–379.

62. Thevenet, F.; Olivier, L.; Batault, F.; Sivachandiran, L.; Locoge, N. Acetaldehyde adsorption on TiO_2: Influence of NO_2 preliminary adsorption. *Chem. Eng. J.* **2015**, *281*, 126–133.

63. Topalian, Z.; Stefanov, B.I.; Granqvist, C.G.; Österlund, L. Adsorption and photo-oxidation of acetaldehyde on TiO_2 and sulfate-modified TiO_2: Studies by in situ FTIR spectroscopy and micro-kinetic modeling. *J. Catal.* **2013**, *307*, 265–274.

64. Idriss, H.; Barteau, M.A. Selectivity and mechanism shifts in the reactions of acetaldehyde on oxidized and reduced TiO_2(001) surfaces. *Catal. Letters* **1996**, *40*, 147–153.

65. Luo, S.; Falconer, J.L. Acetone and Acetaldehyde Oligomerization on TiO_2 Surfaces. *J. Catal.* **1999**, *185*, 393–407.

66. Luo, S.; Falconer, J.L. Aldol condensation of acetaldehyde to form high molecular weight compounds on TiO_2. *Cataysis Lett.* **1999**, *57*, 89–93.

67. Idriss, H.; Pierce, K.; Barteau, M.A. Carbonyl coupling on the titanium dioxide TiO_2(001) surface. *J. Am. Chem. Soc.* **1991**, *113*, 715–716.

68. Thomas, A.G.; Syres, K.L. Adsorption of organic molecules on rutile TiO_2 and anatase TiO_2 single crystal surfaces. *Chem. Soc. Rev.* **2012**, *41*, 4207.

69. Hussain, H.; Torrelles, X.; Cabailh, G.; Rajput, P.; Lindsay, R.; Bikondoa, O.; Tillotson, M.; Grau-Crespo, R.; Zegenhagen, J.; Thornton, G. Quantitative Structure of an Acetate Dye Molecule Analogue at the TiO_2–Acetic Acid Interface. *J. Phys. Chem. C* **2016**, *120*, 7586–7590.

70. Sayago, D.I.; Polcik, M.; Lindsay, R.; Toomes, R.L.; Hoeft, J.T.; Kittel, M.; Woodruff, D.P. Structure Determination of Formic Acid Reaction Products on TiO_2(110). *J. Phys. Chem. B* **2004**, *108*, 14316–14323.

71. Onishi, H.; Iwasawa, Y. STM-imaging of formate intermediates adsorbed on a TiO_2(110) surface. *Chem. Phys. Lett.* **1994**, *226*, 111–114.

72. Thevuthasan, S.; Herman, G.; Kim, Y.; Chambers, S.; Peden, C.H.; Wang, Z.; Ynzunza, R.; Tober, E.; Morais, J.; Fadley, C. The structure of formate on TiO_2(110) by scanned-energy and scanned-angle photoelectron diffraction. *Surf. Sci.* **1998**, *401*, 261–268.

73. Käckell, P.; Terakura, K. Dissociative adsorption of formic acid and diffusion of formate on the TiO_2(110) surface: the role of hydrogen. *Surf. Sci.* **2000**, *461*, 191–198.

74. Tanner, R.E.; Liang, Y.; Altman, E.I. Structure and chemical reactivity of adsorbed carboxylic acids on anatase TiO_2. *Surf. Sci.* **2002**, *506*, 251–271.

75. Altman, E.I.; Tanner, R.E. Using scanning tunneling microscopy to characterize adsorbates

and reactive intermediates on transition metal oxide surfaces. *Catal. Today* **2003**, *85*, 101–111.

76. Yu, Y.-Y.; Gong, X.Q. Unique adsorption behaviors of carboxylic acids at rutile TiO_2(110). *Surf. Sci.* **2015**, *641*, 82–90.

77. Grinter, D.C.; Nicotra, M.; Thornton, G. Acetic Acid Adsorption on Anatase TiO_2(101). *J. Phys. Chem. C* **2012**, *116*, 11643–11651.

78. Foster, A.S.; Nieminen, R.M. Adsorption of acetic and trifluoroacetic acid on the TiO_2(110) surface. *J. Chem. Phys.* **2004**, *121*, 9039–9042.

79. McGill, P.R.; Idriss, H. DFT study of carboxylic acids modes of adsorption on rutile TiO_2(011) surfaces. *Surf. Sci.* **2008**, *602*, 3688–3695.

80. Onishi, H.; Iwasawa, Y. STM observation of surface reactions on a metal oxide. *Surf. Sci.* **1996**, *357–358*, 773–776.

81. Quah, E.L.; Wilson, J.N.; Idriss, H. Photoreaction of the Rutile TiO_2 (011) Single-Crystal Surface: Reaction with Acetic Acid. *Langmuir* **2010**, *26*, 6411–6417.

82. Pichat, P. Some views about indoor air photocatalytic treatment using TiO_2: Conceptualization of humidity effects, active oxygen species, problem of C_1–C_3 carbonyl pollutants. *Appl. Catal. B Environ.* **2010**, *99*, 428–434.

83. Kershis, M.D.; White, M.G. Photooxidation of ethanol and 2-propanol on TiO_2(110): evidence for methyl radical ejection. *Phys. Chem. Chem. Phys.* **2013**, *15*, 17976.

84. Vorontsov, A.; Savinov, E.; Barannik, G..; Troitsky, V.; Parmon, V. Quantitative studies on the heterogeneous gas-phase photooxidation of CO and simple VOCs by air over TiO_2. *Catal. Today* **1997**, *39*, 207–218.

85. Sauer, M.L.; Ollis, D.F. Photocatalyzed Oxidation of Ethanol and Acetaldehyde in Humidified Air. *J. Catal.* **1996**, *158*, 570–582.

86. Sivachandiran, L.; Thevenet, F.; Gravejat, P.; Rousseau, A. Investigation of NO and NO_2 adsorption mechanisms on TiO_2 at room temperature. *Appl. Catal. B Environ.* **2013**, *142–143*, 196–204.

87. Hadjiivanov, K.; Bushev, V.; Kantcheva, M.; Klissurski, D. Infrared spectroscopy study of the species arising during nitrogen dioxide adsorption on titania (anatase). *Langmuir* **1994**, *10*, 464–471.

88. Walenta, C.A.; Kollmannsberger, S.L.; Kiermaier, J.; Winbauer, A.; Tschurl, M.; Heiz, U. Ethanol photocatalysis on rutile TiO_2(110): the role of defects and water. *Phys. Chem. Chem. Phys.* **2015**, *17*, 22809–22814.

89. Zhang, H.; Zhou, P.; Ji, H.; Ma, W.; Chen, C.; Zhao, J. Enhancement of photocatalytic decarboxylation on TiO_2 by water-induced change in adsorption-mode. *Appl. Catal. B Environ.* **2018**, *224*, 376–382.

90. Backes, M.J.; Lukaski, A.C.; Muggli, D.S. Active sites and effects of H_2O and temperature on the photocatalytic oxidation of ^{13}C-acetic acid on TiO_2. *Appl. Catal. B Environ.* **2005**, *61*, 21–35.

91. Liao, L.; Lien, C.; Lin, J. FTIR study of adsorption and photoreactions of acetic acid on TiO_2. *Phys. Chem. Chem. Phys.* **2001**, *3*, 3831–3837.

92. Miller, K.L.; Falconer, J.L.; Medlin, J.W. Effect of water on the adsorbed structure of formic acid on TiO_2 anatase (101). *J. Catal.* **2011**, *278*, 321–328.

93. Hasan, M.A.; Zaki, M.I.; Pasupulety, L. Oxide-catalyzed conversion of acetic acid into acetone: an FTIR spectroscopic investigation. *Appl. Catal. A Gen.* **2003**, *243*, 81–92.

94. Ngo, S.; Betts, L.M.; Dappozze, F.; Ponczek, M.; George, C.; Guillard, C. Kinetics and mechanism of the photocatalytic degradation of acetic acid in absence or presence of O_2. *J. Photochem. Photobiol. A Chem.* **2017**, *339*, 80–88.

95. Piera, E.; Ayllón, J.A.; Doménech, X.; Peral, J. TiO_2 deactivation during gas-phase photocatalytic oxidation of ethanol. *Catal. Today* **2002**, *76*, 259–270.

96. Falconer, J.L.; Magrini-Bair, K.A. Photocatalytic and Thermal Catalytic Oxidation of Acetaldehyde on Pt/TiO_2. *J. Catal.* **1998**, *179*, 171–178.

97. Kim, H.; Choi, W. Effects of surface fluorination of TiO_2 on photocatalytic oxidation of gaseous acetaldehyde. *Appl. Catal. B Environ.* **2007**, *69*, 127–132.

98. Muggli, D.S.; Keyser, S. a; Falconer, J.L. Photocatalytic decomposition of acetic acid on TiO_2. *Catal. Letters* **1998**, *55*, 129–132.

99. Xu, C.; Yang, W.; Guo, Q.; Dai, D.; Yang, X. Photoinduced decomposition of acetaldehyde on a reduced $TiO_2(110)$ surface: involvement of lattice oxygen. *Phys. Chem. Chem. Phys.* **2016**, *18*, 30982–30989.

100. Lee, G.D.; Tuan, V.A.; Falconer, J.L. Photocatalytic Oxidation and Decomposition of Acetic Acid on Titanium Silicalite. *Environ. Sci. Technol.* **2001**, *35*, 1252–1258.

101. Hwang, S.J.; Raftery, D. In situ solid-state NMR studies of ethanol photocatalysis: characterization of surface sites and their reactivities. *Catal. Today* **1999**, *49*, 353–361.

102. Nosaka, Y.; Koenuma, K.; Ushida, K.; Kira, A. Reaction Mechanism of the Decomposition of Acetic Acid on Illuminated TiO_2 Powder Studied by Means of in Situ Electron Spin Resonance Measurements. *Langmuir* **1996**, *12*, 736–738.

103. Murdoch, M.; Waterhouse, G.I.N.; Nadeem, M.A.; Metson, J.B.; Keane, M.A.; Howe, R.F.; Llorca, J.; Idriss, H. The effect of gold loading and particle size on photocatalytic hydrogen production from ethanol over Au/TiO_2 nanoparticles. *Nat. Chem.* **2011**, *3*, 489–492.

104. Rimoldi, L.; Ambrosi, C.; Di Liberto, G.; Lo Presti, L.; Ceotto, M.; Oliva, C.; Meroni, D.; Cappelli, S.; Cappelletti, G.; Soliveri, G.; et al. Impregnation versus Bulk Synthesis: How the Synthetic Route Affects the Photocatalytic Efficiency of Nb/Ta:N Codoped TiO_2 Nanomaterials. *J. Phys. Chem. C* **2015**, *119*, 24104–24115.

105. Nimlos, M.R.; Wolfrum, E.J.; Brewer, M.L.; Fennell, J.A.; Bintner, G. Gas-Phase Heterogeneous Photocatalytic Oxidation of Ethanol: Pathways and Kinetic Modeling. *Environ. Sci. Technol.* **1996**, *30*, 3102–3110.

106. Yu, Z.; Chuang, S. In situ IR study of adsorbed species and photogenerated electrons during photocatalytic oxidation of ethanol on TiO_2. *J. Catal.* **2007**, *246*, 118–126.

107. Meroni, D.; Ardizzone, S.; Cappelletti, G.; Oliva, C.; Ceotto, M.; Poelman, D.; Poelman, H. Photocatalytic removal of ethanol and acetaldehyde by N-promoted TiO_2 films: The role of the different nitrogen sources. *Catal. Today* **2011**, *161*, 169–174.

108. Coronado, J.M.; Kataoka, S.; Tejedor-Tejedor, I.; Anderson, M.A. Dynamic phenomena during the photocatalytic oxidation of ethanol and acetone over nanocrystalline TiO_2: simultaneous FTIR analysis of gas and surface species. *J. Catal.* **2003**, *219*, 219–230.

109. Rimoldi, L.; Giordana, A.; Cerrato, G.; Falletta, E.; Meroni, D. Insights on the photocatalytic degradation processes supported by TiO_2/WO_3 systems. The case of ethanol and tetracycline. *Catal. Today* **2018**.

110. Li, B.; Zhao, J.; Onda, K.; Jordan, K.D.; Yang, J.; Petek, H. Ultrafast Interfacial Proton-Coupled Electron Transfer. *Science (80).* **2006**, *311*, 1436–1440.

111. Tamaki, Y.; Furube, A.; Murai, M.; Hara, K.; Katoh, R.; Tachiya, M. Direct Observation of Reactive Trapped Holes in TiO_2 Undergoing Photocatalytic Oxidation of Adsorbed Alcohols: Evaluation of the Reaction Rates and Yields. *J. Am. Chem. Soc.* **2006**, *128*, 416–417.

112. Yamakata, A.; Ishibashi, T.; Onishi, H. Electron- and Hole-Capture Reactions on Pt/TiO_2 Photocatalyst Exposed to Methanol Vapor Studied with Time-Resolved Infrared Absorption Spectroscopy. *J. Phys. Chem. B* **2002**, *106*, 9122–9125.

113. Shen, M.; Henderson, M.A. Identification of the Active Species in Photochemical Hole Scavenging Reactions of Methanol on TiO_2. *J. Phys. Chem. Lett.* **2011**, *2*, 2707–2710.

114. Muggli, D.S.; McCue, J.T.; Falconer, J.L. Mechanism of the Photocatalytic Oxidation of Ethanol on TiO_2. *J. Catal.* **1998**, *173*, 470–483.

115. Muggli, D.S.; Lowery, K.H.; Falconer, J.L. Identification of Adsorbed Species during Steady-State Photocatalytic Oxidation of Ethanol on TiO_2. *J. Catal.* **1998**, *180*, 111–122.

116. Muggli, D.S.; Larson, S.A.; Falconer, J.L. Photocatalytic Oxidation of Ethanol: Isotopic Labeling and Transient Reaction. *J. Phys. Chem.* **1996**, *100*, 15886–15889.

117. Sopyan, I.; Watanabe, M.; Murasawa, S.; Hashimoto, K.; Fujishima, A. An efficient TiO_2 thin-film photocatalyst: photocatalytic properties in gas-phase acetaldehyde degradation. *J. Photochem. Photobiol. A Chem.* **1996**, *98*, 79–86.

118. Hu, H.; Xiao, W.; Yuan, J.; Shi, J.; Chen, M.; Shang Guan, W. Preparations of TiO_2 film coated on foam nickel substrate by sol-gel processes and its photocatalytic activity for degradation of acetaldehyde. *J. Environ. Sci.* **2007**, *19*, 80–85.

119. Obuchi, E.; Sakamoto, T.; Nakano, K.; Shiraishi, F. Photocatalytic decomposition of acetaldehyde over TiO_2/SiO_2 catalyst. *Chem. Eng. Sci.* **1999**, *54*, 1525–1530.

120. Wilson, D.P.; Sporleder, D.; White, M.G. Final state distributions of methyl radical desorption from ketone photooxidation on TiO_2(110). *Phys. Chem. Chem. Phys.* **2012**, *14*, 13630.

121. Sieland, F.; Schneider, J.; Bahnemann, D.W. Photocatalytic activity and charge carrier dynamics of TiO_2 powders with a binary particle size distribution. *Phys. Chem. Chem. Phys.* **2018**, *20*, 8119–8132.

122. Ohko, Y.; Tryk, D.A.; Hashimoto, K.; Fujishima, A. Autoxidation of Acetaldehyde Initiated

by TiO_2 Photocatalysis under Weak UV Illumination. *J. Phys. Chem. B* **1998**, *102*, 2699–2704.

123. Takeuchi, M.; Deguchi, J.; Sakai, S.; Anpo, M. Effect of H_2O vapor addition on the photocatalytic oxidation of ethanol, acetaldehyde and acetic acid in the gas phase on TiO2 semiconductor powders. *Appl. Catal. B Environ.* **2010**, *96*, 218–223.

124. Kraeutler, B.; Bard, A.J. Photoelectrosynthesis of ethane from acetate ion at an n-type titanium dioxide electrode. The photo-Kolbe reaction. *J. Am. Chem. Soc.* **1977**, *99*, 7729–7731.

125. Heciak, A.; Morawski, A.W.; Grzmil, B.; Mozia, S. Cu-modified TiO_2 photocatalysts for decomposition of acetic acid with simultaneous formation of C_1–C_3 hydrocarbons and hydrogen. *Appl. Catal. B Environ.* **2013**, *140–141*, 108–114.

126. Anthony Byrne, J.; Eggins, B.R.; Dunlop, P.S.M.; Linquette-Mailley, S. The effect of hole acceptors on the photocurrent response of particulate TiO_2 anodes. *Analyst* **1998**, *123*, 2007–2012.

127. Sato, S. Photo-Kolbe reaction at gas-solid interfaces. *J. Phys. Chem.* **1983**, *87*, 3531–3537.

128. Henderson, M.A. A surface science perspective on TiO_2 photocatalysis. *Surf. Sci. Rep.* **2011**, *66*, 185–297.

129. Muggli, D.S.; Falconer, J.L. UV-Enhanced Exchange of O_2 with H_2O Adsorbed on TiO_2. *J. Catal.* **1999**, *181*, 155–159.

130. Henderson, M.A.; Epling, W.S.; Perkins, C.L.; Peden, C.H.F.; Diebold, U. Interaction of Molecular Oxygen with the Vacuum-Annealed TiO_2 (110) Surface: Molecular and Dissociative Channels. *J. Phys. Chem. B* **1999**, *103*, 5328–5337.

131. Henderson, M.A. Acetone Chemistry on Oxidized and Reduced TiO_2 (110). *J. Phys. Chem. B* **2004**, *108*, 18932–18941.

132. Kraeutler, B.; Bard, A.J. Heterogeneous photocatalytic decomposition of saturated carboxylic acids on titanium dioxide powder. Decarboxylative route to alkanes. *J. Am. Chem. Soc.* **1978**, *100*, 5985–5992.

133. Saqlain, S.; Cha, B.J.; Kim, S.Y.; Sung, J.Y.; Choi, M.C.; Seo, H.O.; Kim, Y.D. Impact of humidity on the removal of volatile organic compounds over Fe loaded TiO_2 under visible light irradiation: Insight into photocatalysis mechanism by operando DRIFTS. *Mater. Today Commun.* **2021**, *26*, 102119.

134. Sano, T.; Negishi, N.; Takeuchi, K.; Matsuzawa, S. Degradation of toluene and acetaldehyde with Pt-loaded TiO_2 catalyst and parabolic trough concentrator. *Sol. Energy* **2004**, *77*, 543–552.

135. Sato, S.; Ueda, K.; Kawasaki, Y.; Nakamura, R. In Situ IR Observation of Surface Species during the Photocatalytic Decomposition of Acetic Acid over TiO_2 Films. *J. Phys. Chem. B* **2002**, *106*, 9054–9058.

136. Bianchi, C.L.; Pirola, C.; Galli, F.; Stucchi, M.; Morandi, S.; Cerrato, G.; Capucci, V. Nano and micro-TiO_2 for the photodegradation of ethanol: experimental data and kinetic modelling. *RSC Adv.* **2015**, *5*, 53419–53425.

137. Muñoz-Batista, M.J.; Ballari, M.M.; Cassano, A.E.; Alfano, O.M.; Kubacka, A.; Fernández-García, M. Ceria promotion of acetaldehyde photo-oxidation in a TiO_2-based catalyst: a spectroscopic and kinetic study. *Catal. Sci. Technol.* **2015**, *5*, 1521–1531.

138. Eufinger, K.; Poelman, D.; Poelman, H.; De Gryse, R.; Marin, G.B. Photocatalytic activity of DC magnetron sputter deposited amorphous TiO_2 thin films. *Appl. Surf. Sci.* **2007**, *254*, 148–152.

139. Yamamoto, A. Preparation of titania foams having an open cellular structure and their application to photocatalysis. *J. Catal.* **2004**, *226*, 462–465.

140. Adjimi, S.; Roux, J.-C.; Sergent, N.; Delpech, F.; Thivel, P. X.; Pera-Titus, M. Photocatalytic oxidation of ethanol using paper-based nano-TiO_2 immobilized on porous silica: A modelling study. *Chem. Eng. J.* **2014**, *251*, 381–391.

141. Ouwehand, J.; Van Eynde, E.; De Canck, E.; Lenaerts, S.; Verberckmoes, A.; Van Der Voort, P. Titania-functionalized diatom frustules as photocatalyst for indoor air purification. *Appl. Catal. B Environ.* **2018**, *226*, 303–310.

142. Kim, S.; Lim, S.K. Preparation of TiO_2-embedded carbon nanofibers and their photocatalytic activity in the oxidation of gaseous acetaldehyde. *Appl. Catal. B Environ.* **2008**, *84*, 16–20.

143. Sabatini, V.; Rimoldi, L.; Tripaldi, L.; Meroni, D.; Farina, H.; Ortenzi, M.; Ardizzone, S. TiO_2-SiO_2-PMMA Terpolymer Floating Device for the Photocatalytic Remediation of Water and Gas Phase Pollutants. *Catalysts* **2018**, *8*, 568.

144. Pei, Z.F.; Ponec, V. On the intermediates of the acetic acid reactions on oxides: an IR study. *Appl. Surf. Sci.* **1996**, *103*, 171–182.

145. Murcia, J.J.; Hidalgo, M.C.; Navío, J.A.; Araña, J.; Doña-Rodríguez, J.M. In situ FT-IR study of the adsorption and photocatalytic oxidation of ethanol over sulfated and metallized TiO_2. *Appl. Catal. B Environ.* **2013**, *142–143*, 205–213.

146. Fraters, B.D.; Amrollahi, R.; Mul, G. How Pt nanoparticles affect TiO_2-induced gas-phase photocatalytic oxidation reactions. *J. Catal.* **2015**, *324*, 119–126.

147. Zeng, Q.; Xie, X.; Wang, X.; Wang, Y.; Lu, G.; Pui, D.Y.H.; Sun, J. Enhanced photocatalytic performance of Ag@TiO_2 for the gaseous acetaldehyde photodegradation under fluorescent lamp. *Chem. Eng. J.* **2018**, *341*, 83–92.

148. Körösi, L.; Papp, S.; Bertóti, I.; Dékány, I. Surface and Bulk Composition, Structure, and Photocatalytic Activity of Phosphate-Modified TiO_2. *Chem. Mater.* **2007**, *19*, 4811–4819.

149. Ghosh, M.; Liu, J.; Chuang, S.S.C.; Jana, S.C. Fabrication of Hierarchical V_2O_5 Nanorods on TiO_2 Nanofibers and Their Enhanced Photocatalytic Activity under Visible Light. *ChemCatChem* **2018**, *10*, 3305–3318.

150. Sannino, D.; Vaiano, V.; Ciambelli, P. Innovative structured VO_x/TiO_2 photocatalysts supported on phosphors for the selective photocatalytic oxidation of ethanol to acetaldehyde. *Catal. Today* **2013**, *205*, 159–167.

151. Lin, W.; Xie, X.; Wang, X.; Wang, Y.; Segets, D.; Sun, J. Efficient adsorption and sustainable degradation of gaseous acetaldehyde and o-xylene using rGO-TiO_2 photocatalyst. *Chem. Eng. J.* **2018**, *349*, 708–718.

152. Araña, J.; Doña-Rodríguez, J.M.; González-Díaz, O.; Tello Rendón, E.; Herrera Melián, J.A.; Colón, G.; Navío, J.A.; Pérez Peña, J. Gas-phase ethanol photocatalytic degradation study with TiO_2 doped with Fe, Pd and Cu. *J. Mol. Catal. A Chem.* **2004**, *215*, 153–160.

153. Kim, D.S.; Kwak, S.-Y. The hydrothermal synthesis of mesoporous TiO_2 with high crystallinity, thermal stability, large surface area, and enhanced photocatalytic activity. *Appl. Catal. A Gen.* **2007**, *323*, 110–118.

154. Verbruggen, S.W.; Masschaele, K.; Moortgat, E.; Korany, T.E.; Hauchecorne, B.; Martens, J.A.; Lenaerts, S. Factors driving the activity of commercial titanium dioxide powders towards gas phase photocatalytic oxidation of acetaldehyde. *Catal. Sci. Technol.* **2012**, *2*, 2311–2318.

155. Rismanchian, A.; Chen, Y.-W.; Chuang, S.S.C. In situ infrared study of photoreaction of ethanol on Au and Ag/TiO_2. *Catal. Today* **2016**, *264*, 16–22.

156. Gonzalez-Yañez, E.O.; Fuentes, G.A.; Hernández-Terán, M.E.; Fierro-Gonzalez, J.C. Influence of supported gold particles on the surface reactions of ethanol on TiO_2. *Appl. Catal. A Gen.* **2013**, *464–465*, 374–383.

157. Boyle, D.T.; Wilke, J.A.; Palomino, R.M.; Lam, V.H.; Schlosser, D.A.; Andahazy, W.J.; Stopak, C.Z.; Stacchiola, D.J.; Rodriguez, J.A.; Baber, A.E. Elucidation of Active Sites for the Reaction of Ethanol on TiO_2/Au(111). *J. Phys. Chem. C* **2017**, *121*, 7794–7802.

158. Kennedy, J.C.; Datye, A.K. Photothermal Heterogeneous Oxidation of Ethanol over Pt/TiO_2. *J. Catal.* **1998**, *179*, 375–389.

159. Zeng, J.; Francia, C.; Dumitrescu, M.A.; Monteverde Videla, A.H.A.; Ijeri, V.S.; Specchia, S.; Spinelli, P. Electrochemical performance of Pt-based catalysts supported on different ordered mesoporous carbons (Pt/OMCs) for oxygen reduction reaction. *Ind. Eng. Chem. Res.* **2012**, *51*, 7500–7509.

160. Kong, L.; Guo, X.; Xu, J.; Mo, Z.; Li, L. Morphology control of WO_3 nanoplate film on W foil by oxalic acid for photocatalytic gaseous acetaldehyde degradation. *J. Photochem. Photobiol. A Chem.* **2020**, *401*, 112760.

161. Jin, Z.; Murakami, N.; Tsubota, T.; Ohno, T. Complete oxidation of acetaldehyde over a composite photocatalyst of graphitic carbon nitride and tungsten(VI) oxide under visible-light irradiation. *Appl. Catal. B Environ.* **2014**, *150–151*, 479–485.

162. Katsumata, K.; Motoyoshi, R.; Matsushita, N.; Okada, K. Preparation of graphitic carbon nitride (g-C_3N_4)/WO_3 composites and enhanced visible-light-driven photodegradation of acetaldehyde gas. *J. Hazard. Mater.* **2013**, *260*, 475–482.

163. Li, C.; Raziq, F.; Liu, C.; Li, Z.; Sun, L.; Jing, L. Enhanced photocatalytic activity for degrading pollutants of g-C_3N_4 by promoting oxygen adsorption after H_3BO_3 modification. *Appl. Surf. Sci.* **2015**, *358*, 240–245.

164. Raziq, F.; Qu, Y.; Humayun, M.; Zada, A.; Yu, H.; Jing, L. Synthesis of SnO_2/B-P codoped g-C_3N_4 nanocomposites as efficient cocatalyst-free visible-light photocatalysts for CO_2 conversion and pollutant degradation. *Appl. Catal. B Environ.* **2017**, *201*, 486–494.

165. Yamaguchi, Y.; Usuki, S.; Yamatoya, K.; Suzuki, N.; Katsumata, K.; Terashima, C.; Fujishima, A.; Kudo, A.; Nakata, K. Efficient photocatalytic degradation of gaseous

acetaldehyde over ground Rh–Sb co-doped $SrTiO_3$ under visible light irradiation. *RSC Adv.* **2018**, *8*, 5331–5337.

166. Pargoletti, E.; Mostoni, S.; Rassu, G.; Pifferi, V.; Meroni, D.; Falciola, L.; Davoli, E.; Marelli, M.; Cappelletti, G. Zn- vs Bi-based oxides for *o*-toluidine photocatalytic treatment under solar light. *Environ. Sci. Pollut. Res.* **2017**, *24*.

167. Dias, L.P.; Correia, F.C.; Ribeiro, J.M.; Tavares, C.J. Photocatalytic Bi_2O_3/TiO_2:N Thin Films with Enhanced Surface Area and Visible Light Activity. *Coatings* **2020**, *10*, 445.

168. Gao, Z.; Wang, J.; Muhammad, Y.; Zhang, Y.; Shah, S.J.; Hu, Y.; Chu, Z.; Zhao, Z.; Zhao, Z. Enhanced moisture-resistance and excellent photocatalytic performance of synchronous N/Zn-decorated MIL-125(Ti) for vaporous acetaldehyde degradation. *Chem. Eng. J.* **2020**, *388*, 124389.

169. Zhang, J.; Hu, Y.; Qin, J.; Yang, Z.; Fu, M. TiO_2-UiO-66-NH_2 nanocomposites as efficient photocatalysts for the oxidation of VOCs. *Chem. Eng. J.* **2020**, *385*, 123814.

170. Fang, X.; Lu, G.; Mahmood, A.; Tang, Z.; Liu, Z.; Zhang, L.; Wang, Y.; Sun, J. A novel ternary Mica/TiO_2/Fe_2O_3 composite pearlescent pigment for the photocatalytic degradation of acetaldehyde. *J. Photochem. Photobiol. A Chem.* **2020**, *400*, 112617.

171. Fang, X.; Lu, G.; Mahmood, A.; Wang, Y.; Wang, X.; Xie, X.; Tang, Z.; Sun, J. A novel ternary mica-titania@rGO composite pearlescent pigment for the photocatalytic degradation of gaseous acetaldehyde. *Chem. Eng. J.* **2020**, *396*, 125312.

172. Peral, J.; Ollis, D.F. TiO_2 photocatalyst deactivation by gas-phase oxidation of heteroatom organics. *J. Mol. Catal. A Chem.* **1997**, *115*, 347–354.

173. Peral, J.; Ollis, D. Heterogeneous photocatalytic oxidation of gas-phase organics for air purification: Acetone, 1-butanol, butyraldehyde, formaldehyde, and m-xylene oxidation. *J. Catal.* **1992**, *136*, 554–565.

174. Destaillats, H.; Sleiman, M.; Sullivan, D.P.; Jacquiod, C.; Sablayrolles, J.; Molins, L. Key parameters influencing the performance of photocatalytic oxidation (PCO) air purification under realistic indoor conditions. *Appl. Catal. B Environ.* **2012**, *128*, 159–170.

175. Lyu, J.; Zhu, L.; Burda, C. Considerations to improve adsorption and photocatalysis of low concentration air pollutants on TiO_2. *Catal. Today* **2014**, *225*, 24–33.

176. Mamaghani, A.H.; Haghighat, F.; Lee, C.-S. Photocatalytic degradation of VOCs on various commercial titanium dioxides: Impact of operating parameters on removal efficiency and by-products generation. *Build. Environ.* **2018**, *138*, 275–282.

177. Héquet, V.; Raillard, C.; Debono, O.; Thévenet, F.; Locoge, N.; Le Coq, L. Photocatalytic oxidation of VOCs at ppb level using a closed-loop reactor: The mixture effect. *Appl. Catal. B Environ.* **2018**, *226*, 473–486.

178. Mamaghani, A.H.; Haghighat, F.; Lee, C.S. Photocatalytic oxidation technology for indoor environment air purification: The state-of-the-art. *Appl. Catal. B Environ.* **2017**, *203*, 247–269.

179. Lugo-Vega, C.S.; Moreira, J.; Serrano-Rosales, B.; De Lasa, H. Kinetics of the pollutant photocatalytic conversion in a Photo-CREC-Air Reactor. *Chem. Eng. J.* **2017**, *317*, 1069–1082.

180. Boyjoo, Y.; Sun, H.; Liu, J.; Pareek, V.K.; Wang, S. A review on photocatalysis for air treatment: From catalyst development to reactor design. *Chem. Eng. J.* **2017**, *310*, 537–559.

181. Van Walsem, J.; Verbruggen, S.W.; Modde, B.; Lenaerts, S.; Denys, S. CFD investigation of a multi-tube photocatalytic reactor in non-steady-state conditions. *Chem. Eng. J.* **2016**, *304*, 808–816.

182. 22197-2:2019, I. Fine ceramics (advanced ceramics, advanced technical ceramics) — Test method for air-purification performance of semiconducting photocatalytic materials — Part 2: Removal of acetaldehyde **2019**, 16.

183. Mills, A.; Hill, C.; Robertson, P.K.J. Overview of the current ISO tests for photocatalytic materials. *J. Photochem. Photobiol. A Chem.* **2012**, *237*, 7–23.

184. AFNOR Norme expérimentale XP B44-13 Méthode d'essais et d'analyse pour la mesure d'efficacité de systèmes photocatalytiques pour l'élimination des composés organiques volatiles/odeurs dans l'air intérieur en recirculation: test en enceinte confinée **2009**.

185. Costarramone, N.; Kartheuser, B.; Pecheyran, C.; Pigot, T.; Lacombe, S. Efficiency and harmfulness of air-purifying photocatalytic commercial devices: From standardized chamber tests to nanoparticles release. *Catal. Today* **2015**, *252*, 35–40.

186. Costarramone, N.; Cantau, C.; Desauziers, V.; Pécheyran, C.; Pigot, T.; Lacombe, S. Photocatalytic air purifiers for indoor air: European standard and pilot room experiments. *Environ. Sci. Pollut. Res.* **2017**, *24*, 12538–12546.

187. Ghislain, M.; Costarramone, N.; Pigot, T.; Reyrolle, M.; Lacombe, S.; Le Bechec, M. High frequency air monitoring by selected ion flow tube-mass spectrometry (SIFT-MS): Influence of the matrix for simultaneous analysis of VOCs, CO_2, ozone and water. *Microchem. J.* **2020**, *153*, 104435.

188. Furukawa, S.; Shishido, T.; Teramura, K.; Tanaka, T. Photocatalytic Oxidation of Alcohols over TiO_2 Covered with Nb_2O_5. *ACS Catal.* **2012**, *2*, 175–179.

189. Araña, J.; Doña-Rodríguez, J.M.; Cabo, C.G. i; González-Díaz, O.; Herrera-Melián, J.A.; Pérez-Peña, J. FTIR study of gas-phase alcohols photocatalytic degradation with TiO_2 and AC-TiO_2. *Appl. Catal. B Environ.* **2004**, *53*, 221–232.

190. Awa, K.; Akashi, R.; Akita, A.; Naya, S.; Kobayashi, H.; Tada, H. Highly Efficient and Selective Oxidation of Ethanol to Acetaldehyde by a Hybrid Photocatalyst Consisting of SnO_2 Nanorod and Rutile TiO_2 with Heteroepitaxial Junction. *ChemPhysChem* **2019**, *20*, 2155–2161.

191. Balayeva, N.O.; Fleisch, M.; Bahnemann, D.W. Surface-grafted WO_3/TiO_2 photocatalysts: Enhanced visible-light activity towards indoor air purification. *Catal. Today* **2018**, *313*, 63–71.

192. Weon, S.; Choi, W. TiO_2 Nanotubes with Open Channels as Deactivation-Resistant Photocatalyst for the Degradation of Volatile Organic Compounds. *Environ. Sci. Technol.* **2016**, *50*, 2556–2563.

193. Wang, X.; Yang, Y.; Lu, G.; Shi, G.; Wang, Y.; Wang, R.; Xie, X.; Sun, J. In-situ preparation of Ti_3C_2/Ti^{3+}-TiO_2 composites with mosaic structures for the adsorption and Photo-degradation of flowing acetaldehyde under visible light. *Appl. Surf. Sci.* **2020**, *531*,

147101.

194. Kong, L.; Zhang, X.; Wang, C.; Xu, J.; Du, X.; Li, L. Ti^{3+} defect mediated g-C_3N_4/TiO_2 Z-scheme system for enhanced photocatalytic redox performance. *Appl. Surf. Sci.* **2018**, *448*, 288–296.

Table 1. Cross sections, defined as the ratio between rate constant (in s^{-1}) and light flux (in number of photons cm^{-2} s^{-1}), reported in the literature for ethanol, acetaldehyde and acetic acid photocatalytic degradation by single-crystal TiO_2 under UV irradiation.

molecule	**surface**	**cross section (cm^2)**	**p_{O2} (torr)**	**Ref.**
ethanol	rutile(110)	2×10^{-18}	1×10^{-6}	[39]
ethanol	anatase(101)	$(4\text{-}1)\times10^{-19}$	$(2.5\text{-}7.5)\times10^{-8}$	[55]
ethanol	rutile(110)	2×10^{-19}*	10^{-7}–10^{-9}	[57]
acetaldehyde	rutile(011)	10^{-17}–10^{-19}	Predosed	[36]
acetaldehyde	rutile(110)	ca. 10^{-22} **	-	[99]
acetic acid	rutile(011)	9×10^{-22}	1×10^{-6}	[81]
acetic acid	rutile(011)	5×10^{-22}	1×10^{-8}	[81]

* For acetaldehyde formation

** Visible-light irradiation (λ >400 nm)

Table 2. A selective overview of TiO_2-based photocatalysts for the degradation of ethanol (EtOH), acetaldehyde (AcH) or acetic acid (AcOH); A:anatase, R:rutile, B:brookite; n.d. = not determined.

photocatalyst		post-treatment	physicochemical properties				test conditions		pollutant	Ref.
			S_{BET} ($m^2\ g^{-1}$)	phase composition (%)	d (nm)	E_g (eV)				
Sol-gel TiO_2	Pristine	calc. (700°C)	6	A 100	>100	2.97	C_0= 12,030 ppm, RH ~70%	UV	EtOH	[148]
	P/Ti = 1%at		10	A 86–R 14	23.7	n.d.				
	P/Ti = 5%at		75	A 82–R 18	11.9	3.13				
	P/Ti=10%at		105	A 75–R 25	9.4	n.d.				
Sol-gel TiO_2	Sulfated	calc. (650°C)	58	A 100	20	n.d.	3:1 v/v EtOH-H_2O	UV	EtOH	[145]
	Au+Sulfated		60		19					
	Pt+Sulfated		49		20					
Hombikat UV100	1%w Pt	vacuum drying	n.d.	A 100	1.5-3.0	n.d.	C_0= 1.1 %v; C_{O2}= 0-19.5%v; RH= 0-40%	UV (LED)	EtOH	[146]
Sol-gel TiO_2	Pristine	calc. (400°C)	149	A–B	10.2	3.23	C_0= 198-238 ppm	UV, simulated solar	EtOH	[104]
	N-doped		132		11.6	3.18				
	Nb-doped		119		12.8	3.09				
	Nb,N-codoped		161		9.5	3.13				
	Ta-doped		135		11.3	3.16				
	Ta,N-codoped		111		13.8	3.09				
	NH_3- impregnated		165		9.3	3.22				
	Nb-impregnated		133		11.5	3.22				
	N,Nb-impregnated		150		10.2	3.22				
	Ta-imprgnated		124		12.3	3.24				
	N,Ta-impregnated		123		12.4	3.23				
Electro-deposited TiO_2 films	-	calc. (400°C)	n.d.	n.d.	n.d.	n.d.	C_0= 140-275 ppm	UV, simulated solar	EtOH	[18]

V_2O_5 nanorods on TiO_2 nanofibers	V_2O_5 fiber	calc. (400-600°C)	8	A 100	-	2.23	EtOH-saturated O_2 stream (15 sccm)	Visible	EtOH	[149]
	V:Ti = 1:1		58		10-25	2.26				
	V:Ti = 1:1		12		25-50	2.24				
	V:Ti = 1:1		10		80-100;	2.30				
	V_2O_5 powder		6		-	2.22				
	TiO_2 fiber		30		13-29	3.23				
	P25 $_{TiO2}$		45		8-21	3.08				
P25 Evonik	Pristine 1% Au 1% Ag	180°C	n.d.	A 80-R 20	n.d.	n.d.	saturated EtOH/Ar gas flow	UV	EtOH	[155]
P25 Evonik	<1% Pt	-	50	A 80-R 20	n.d.	n.d.	n.d.	UV	EtOH	[158]
P25 Evonik	Pristine 7% activated carbon	-	50 90	A 80-R 20	n.d.	n.d.	7.2 µmol/min	UV	EtOH	[189]
Commercial TiO_2 powders	P25 Evonik	-	52	A 80-R 20	26	3.21	C_0= 400 ppm; RH= 40%	UV	EtOH	[22]
	Krono 1077		11	A 100	130	3.15				
	A-HR Hunsdman		12	A 100	130	3.15				
SnO_2 nanorods-TiO_2	-	-	7	R 100	n.d.	3.70	C_0= 172 µmol	UV (Xe lamp, 300 W)	EtOH	[190]
WO_3/TiO_2	4% Ti/W	calc (450°C)	151	A 65–B 35	7	3.23	C_0= 198 ppm	UV	EtOH	[109]
	6% Ti/W		158	A 64–B 36	6	3.23				
	8% Ti/W		170	A 68–B 32	6	3.24				
TiO_2 on ZnS based phosphors microparticles	10%w Ti	calc. (400°C)	10	A 100	19	3.2	C_0= 0.2-2 %v, He stream, O_2/EtOH ratio = 2	UV (LED)	EtOH, AcH	[150]
	20%w Ti		13		24	3.2				
	30%w Ti		19		26	3.2				
	5%w V_2O_5-10%w Ti		6		28	2.8				
	5%w V_2O_5-20%w Ti		15		25	2.7				
	5%w V_2O_5-30%w Ti		20		27	2.8				
Sol-gel TiO_2	Pristine	calc. (400°C)	173	A 100	7	3.25	C_0(EtOH) = 273 ppm; C_0(AcH) = 300 ppm	UV for EtOH; UV and solar for AcH	EtOH, AcH	[107]
	N-doped TiO_2 (trietilamine)		104		9	3.19				
	N-doped TiO_2 (NH_3)		120		15	2.98				
	N-doped TiO_2 (NH_3, precipitation)		98		17	3.08				

Ag nanowires@TiO_2	Pristine Ag/Ti 25% Ag/Ti 50% Ag/Ti 75%	autoclave (160°C)	112 109 106 100	A 100	n.d.	n.d.	C_0= 500 ppm, flow rate= 20 sccm	Fluorescent lamp	AcH	[147]
P25 Evonik	stabilized by diatom frustules	calc. (550°C)	85	A 100	12	n.d.	flow rate= 400 cm^3 min^{-1}	UV	AcH	[141]
P25 Evonik	0.5% rGO	autoclave (433 K)	227	A 100	8-10	n.d.	C_0= 25 ppm, dry air	UV	AcH	[151]
Commercial TiO_2 paste	Pristine Sulfated	calc. (450°C)	69	n.d.	n.d.	n.d.	C_0= 50 ppm	UV	AcH	[63]
Flame pyrolysis TiO_2	fluorination	-	n.d.	n.d.	n.d.	n.d.	C_0= 50 µmol	UV	AcH	[42]
Fe(III) grafted WO_3/TiO_2	2.5%w WO_3	calc. (500°C)	42	A – R	5-7 nm	2.90	C_0= 200 ppm	UV	AcH	[191]
	0.005% Fe - 2.5%w WO_3	-	50			<2.90				
	0.1% Fe - 2.5%w WO_3		58							
	0.2% Fe - 2.5%w WO_3		44							
	0.3% Fe - 2.5%w WO_3									
TiO_2 open channels nanotubes	-	calc. (450°C)	n.d.	A 100	n.d.	n.d.	C_0= 1000 ppmv, RH= 65%	UV (LED)	AcH	[192]
{001}-TiO_2 filter	-	calc. (400°C)	n.d.	A 100	10-20	2.95	C_0= 1000 ppmv, RH= 65%	UV (LED)	AcH	[13]
TiO_2-UiO-66-NH_2	75% TiO_2 – 25% UiO-66-NH_2	-	281	A – R	n.d.	ca. 2.90	C_0= 25 ppm	UV (LED)	AcH	[169]
Ti_3C_2/Ti^{3+}-TiO_2	-	-	125	A 100	n.d.	n.d.	C_0= 500 ppm	UV (Xe lamp, 500 W)	AcH	[193]
g-C_3N_4/Ti^{3+}-doped TiO_2 Z-scheme	-	calc. (350°C, H_2/Ar)	63	A 100	n.d.	2.80	C_0= 200 ppm	Simulated solar light (Xe lamp, 150 W)	AcH	[194]
Evonik P25 and Hombikat UV100	Pristine Pt/TiO_2	-	n.d.	n.d.	n.d.	n.d.	C_0= 0.1 mol L^{-1}	UV	AcOH	[102]

Table 3. Emerging photocatalysts used for the gas-phase degradation of acetaldehyde; n.d. = not determined.

photocatalyst		physicochemical properties			test conditions		Ref.
		S_{BET} (m^2 g^{-1})	d (nm)	E_g (eV)			
Mica-TiO_2-rGO	MT@rGO-0.10	17	10-20	2.85	C_0= 500 ppm	UV (Xe lamp, 400 W)	[171]
Mica-TiO_2-Fe_2O_3	MTF 1.5% (Fe/Ti)	44	n.d.	3.00	C_0= 500 ppm	UV (Xe lamp, 400 W)	[170]
N/Zn-codoped MIL-125(Ti)	MIL-125(N-Ti_9Zn_1)	1420	n.d.	1.85	C_0= 200 ppm, RH = 80%	UV (Xe lamp, 400 W)	[168]
H_3BO_3-modified g-C_3N_4	B/N 1% B/N 3% B/N 5% B/N 7%	6	n.d.	2.70	C_0= 810 ppm, 20% O_2	Xe lamp, 150 W	[163]
g-C_3N_4/WO_3	g-C_3N_4/WO_3 8/2	6	n.d.	2.73	C_0= 250 ppm, RH= 50%	Fluorescent lamp	[162]
	g-C_3N_4/WO_3 6/4	5		2.73			
	g-C_3N_4/WO_3 4/6	5		2.75			
	g-C_3N_4/WO_3 2/8	4		2.73			
WO_3 nanoplate film	-	n.d.	19	2.58	C_0= 2% in N_2	Simulated solar light (Xe lamp, 150 W)	[160]
SnO_2/B-P-codoped g-C_3N_4	6SnO_2/0.12B-0.20P-CN	n.d.	n.d.	2.20	C_0= 810 ppm, 20% O_2	Sunlight (Xe lamp, 150 W)	[164]
Rh–Sb-codoped $SrTiO_3$	Rh(1%),Sb(1%)	47	n.d.	n.d.	C_0= 150 ppm, RH= 50%	Visible light (Xe lamp, 200 W)	[165]

Figure Captions

Figure 1. Overview of the topics covered in the review highlighting the interconnected key factors regarding VOCs photoremoval.

Figure 2. (a) STM image of a TiO_2 rutile(110) surface after exposure to ethanol at 145 K followed by annealing at 280 K; assignments of the adsorbates are given in (b). Squares, hexagons, and circles indicate O_{br} vacancies, single H adatoms and paired H adatoms, respectively. (b) STM height histograms of the distinct adsorbates observed in STM images. (c-f) Adsorption geometries and corresponding adsorption energies of the most stable configurations of molecularly (c,e) and dissociatively (d,f) adsorbed ethanol on rutile(110): adsorption at an O_{br} vacancy (c,d); configurations without O_{br} vacancies (e,f); red, dark gray, black, yellow and pink spheres represent Ti_{5c}, O_{br}, C, H and $O_{ethanol}$ atoms, respectively. Adapted from Ref.[48] with permission of the American Physical Society.

Figure 3. UPS valence band spectra of TiO_2(110) taken after O_2 dose and subsequent ethanol dose at RT. Reproduced from Ref.[40] with permission of Elsevier.

Figure 4. Adsorption geometries of acetaldehyde on rutile(110) TiO_2: adsorption on top of a Ti_{5c} site on a stoichiometric surface (a); at an oxygen vacancy on a reduced surface (c). Geometries of adsorption for O-acetaldehyde complex on rutile(110): after coordination to an O_{ad} adatom on an oxidized surface (b); after coordination to an O_2 molecule adsorbed on an oxygen vacancy (d). Adapted from Ref.[45] with permission of the American Chemical Society.

Figure 5 – (a) Most stable adsorption geometry of acetaldehyde on anatase(001) surface. Light gray, red, dark gray and blue spheres are titanium, oxygen, carbon and hydrogen atoms, respectively. Original bond lengths (in Å) are reported in parentheses. (b) Corresponding charge density difference between the clean TiO_2 surface, gas-phase acetaldehyde and the surface with adsorbed acetaldehyde. Yellow spots represent areas gaining electrons, while blue ones represent areas losing electrons Adapted from Ref.[46] with permission of the American Chemical Society.

Figure 6. Scheme of aldol condensation reactions of acetaldehyde molecules adsorbed on TiO_2; reproduced from Ref.[58] with permission of Elsevier.

Figure 7. Acetic acid adsorption in bidentate bridge geometry on a rutile(110)-(2×1) surface. Blue, red, black, small pink spheres are oxygen, titanium, carbon, and hydrogen atoms, respectively. Reproduced from Ref.[69] with permission of the American Chemical Society.

Figure 8. STM images of rutile(110) at RT: (a) clean surface (an O_{vac} is highlighted by a circle); after adsorption of 0.04 ML (b) and 0.43 ML (c) acetate; (d) saturation coverage with

acetate overlayer arranged in a (2×1) superstructure. Reprinted from Ref.[51] with permission of the American Chemical Society.

Figure 9. Irreversibly adsorbed acetaldehyde fractions on TiO_2 (q_{irr}) as a function of NO_x surface coverage, θ, under dry air at 296 K. Reproduced from Ref.[62] with permission of Elsevier.

Figure 10. (a,b) Adsorption geometries of acetic acid on anatase(101) surface with co-adsorbed water: water molecule placed far away (a) and near (b) the acetic acid molecule. The iso-surfaces represent spin-density distributions in the presence of an extra hole. (c) The projected density of states (PDOS) of different potential hole trapping sites on anatase(101). Dashed lines represent the total DOS of the corresponding slabs. DOS are aligned with Ti 3s states in the middle of the slabs. (d) Switching of acetic acid adsorption mode between bridged bidentate to monodentate coordination in the presence of water. Adapted from Ref.[89] with permission of Elsevier.

Figure 11. Photocatalytic degradation pathway of ethanol as proposed in Ref.[85]; reproduced with permission of Elsevier.

Figure 12. (a) Energy profiles for photocatalytic oxidation of adsorbed ethanol on stoichiometric rutile(110) supercell with an OH group adsorbed on one side (energies in eV). Formation of Ti-bound ethoxide (b) and of acetaldehyde (c), with corresponding band schemes. Filling of the bands and the Fermi level (E_F) are indicated by dark yellow colour and a dashed line, respectively. Atoms of Ti_{5c}, O_{br}, in-plane O, C, H_{ad} and ethanol oxygen are represented in red-brown, dark-grey, light-grey, black, yellow and pink, respectively. Reproduced from Ref.[26] with permission of Nature.

Figure 13. Photocatalytic degradation pathway of acetaldehyde as proposed in Ref.[29]; reproduced with permission of Elsevier.

Figure 14. Relative concentration of intermediates of photocatalytic oxidation of acetic acid over TiO_2 under UV irradiation in the presence of O_2 and photocatalytic degradation pathway of acetic acid as proposed in Ref.[91]; reproduced with permission of the Royal Society of Chemistry.

Figure 15. (a) Difference FTIR spectra of adsorbed species and CO_2 during photocatalytic oxidation of adsorbed ethanol on P25 TiO_2 with O_2 pulses; (b) Variation of the coverage of adsorbed species as a function of UV illumination time. The dotted line represents the cumulative coverage of O_{2ad}, and the continuous black line the resulting IR intensity at 2000 cm^{-1} (I_{2000}) after each O_2 addition; reproduced from Ref.[30] with permission of the American Chemical Society.

Figure 16. Effect of water vapor addition on the photocatalytic oxidation on TiO_2 of acetaldehyde (a), acetic acid (b) and ethanol (c) under UV irradiation. Reprinted from Ref.[123] with permission of Elsevier.

Figure 17. Proposed mechanism of photothermal oxidation of ethanol by Au/TiO_2; Black arrows represent associated electron transfer steps, while red and blue highlights indicate plasmonically-mediated charge transfer and bandgap photoexcitation, respectively. Reprinted from Ref.[31] with permission of the American Chemical Society.

Figure 18. Performance of a flat TiO_2-coated filter working in recirculating mode towards the removal of a mixture of pollutants from a 20 m^3-test chamber with an air exchange rate of 1 h^{-1} using UVC irradiation: global chamber removal efficiency for each pollutant (final-to-initial pollutant concentration ratio, C_{ss}/C_0) as a function of recirculation flow; reprinted from Ref.[174] with permission of Elsevier**.**

Figure 19. Relationship between by-product concentrations and several parameters during ethanol photocatalytic degradation in a pilot duct system under UV irradiation: ethanol inlet concentration (a), airflow (b), RH (c), light intensity (d); adapted from Ref.[14] with permission of Elsevier**.**

Figure 20. (a) Airflow rate profile modeled by CFD in a multi-tube photoreactor (scale in m s^{-1}); b) Acetaldehyde transient concentrations in the P25 TiO_2-coated reactor under UV illumination for three different initial pollutant concentrations (colored dots) and concentration profiles simulated by CFD modeling (black lines). Reproduced from Ref. [181] with permission of Elsevier.

Figure 21. (a) Photo and cross-sectional FE-SEM image (inset) of a TiO_2 nanotube filter (TNT); (b) filter unit containing also a reflector plate; (c) inside view of a Samsung AX7000 air cleaner equipped with two TNT filters and UV-LEDs; (d) test chamber; reprinted from Ref.[13] with permission of the American Chemical Society.

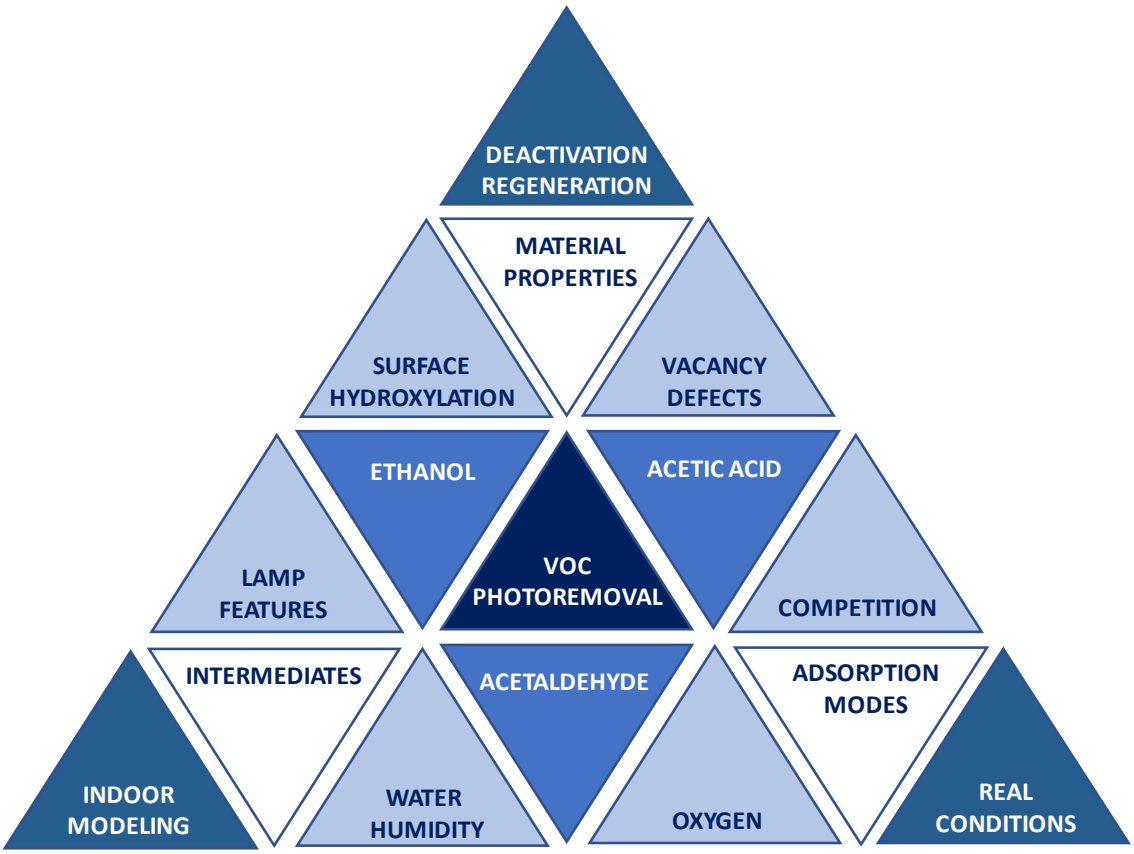
DEACTIVATION
REGENERATION
MATERIAL
PROPERTIES
SURFACE
HYDROXYLATION
VACANCY
DEFECTS
ETHANOL
ACETIC ACID
LAMP
FEATURES
VOC
PHOTOREMOVAL
COMPETITION
INTERMEDIATES
ACETALDEHYDE
ADSORPTION
MODES
INDOOR
MODELING
WATER
HUMIDITY
OXYGEN
REAL
CONDITIONS

FIGURE 1

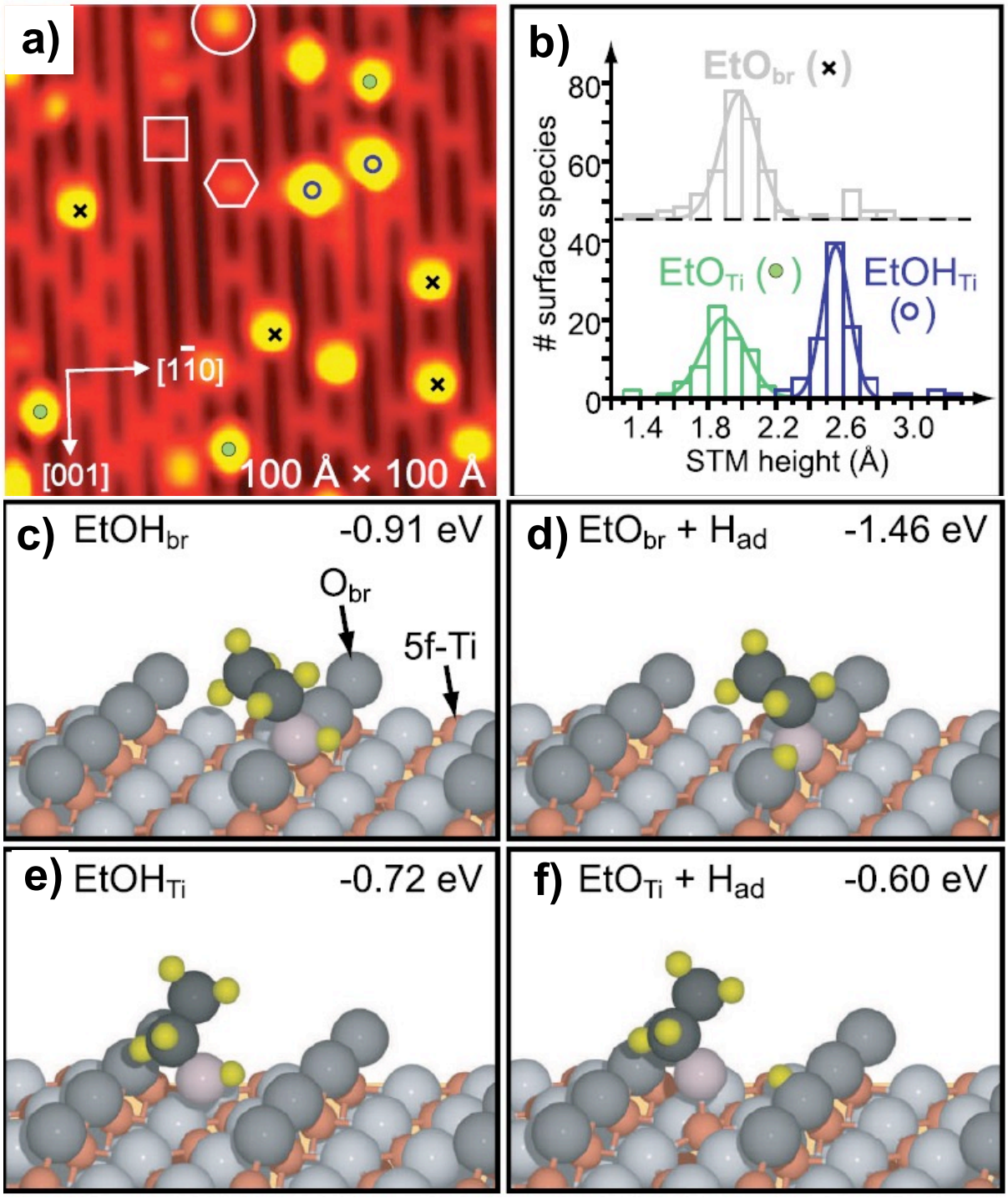
a)
[1$\bar{1}$0]
[001]
100 Å × 100 Å
b)
EtO$_{br}$ (×)
surface species
80
60
40
20
0
EtO$_{Ti}$ (●)
EtOH$_{Ti}$ (○)
1.4 1.8 2.2 2.6 3.0
STM height (Å)
c) EtOH$_{br}$ -0.91 eV
O$_{br}$
5f-Ti
d) EtO$_{br}$ + H$_{ad}$ -1.46 eV
e) EtOH$_{Ti}$ -0.72 eV
f) EtO$_{Ti}$ + H$_{ad}$ -0.60 eV

FIGURE 2

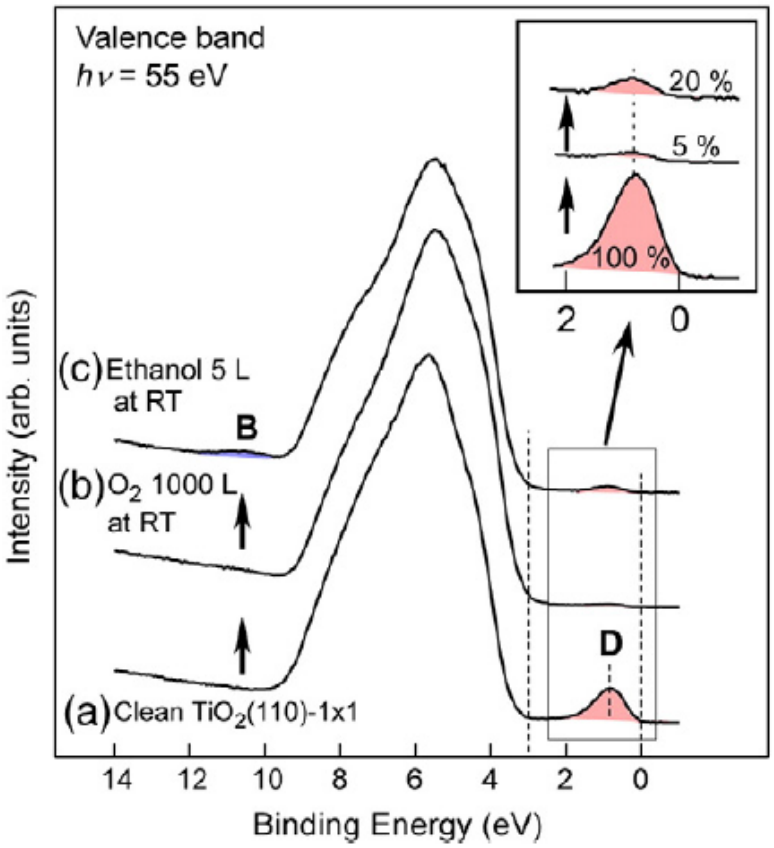
Valence band
hν = 55 eV
20 %
5 %
100 %
2
0
(c) Ethanol 5 L
at RT
B
(b) O2 1000 L
at RT
D
(a) Clean TiO2(110)-1x1
Intensity (arb. units)
14
12
10
8
6
4
2
0
Binding Energy (eV)

FIGURE 3

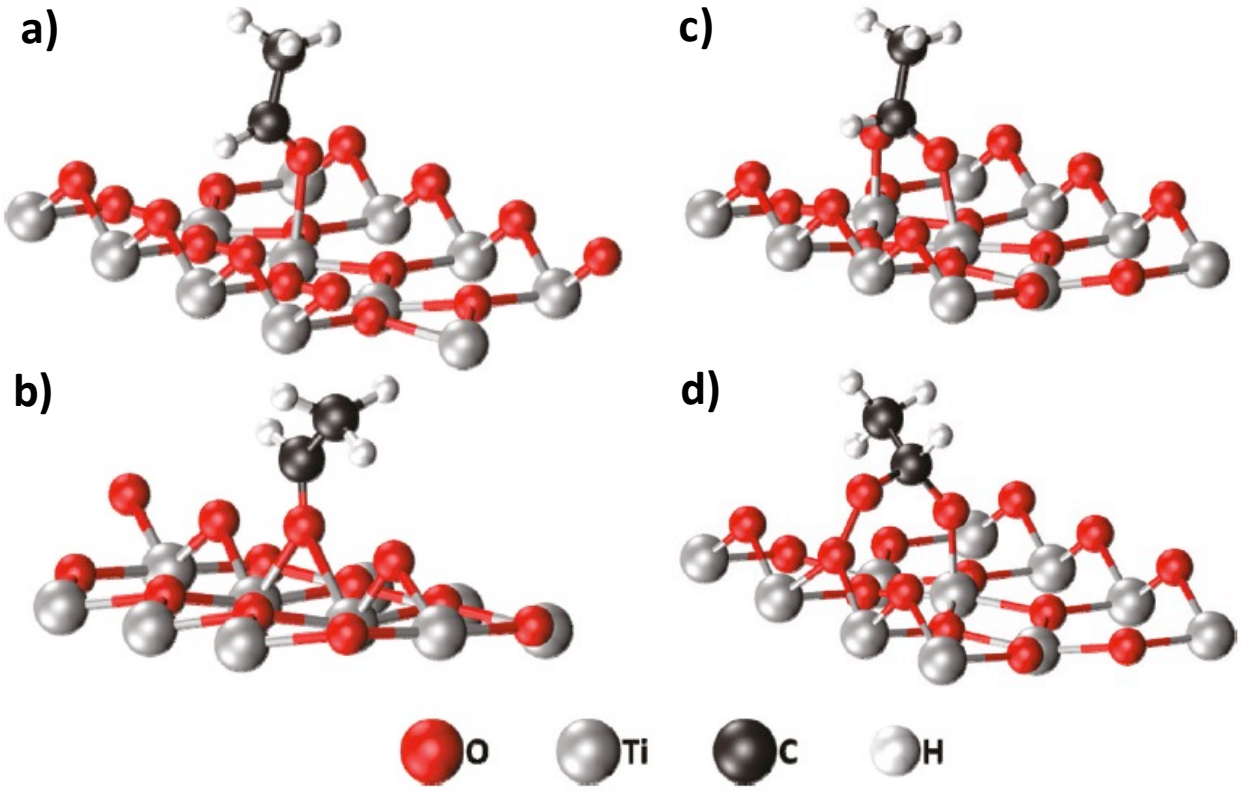

FIGURE 4

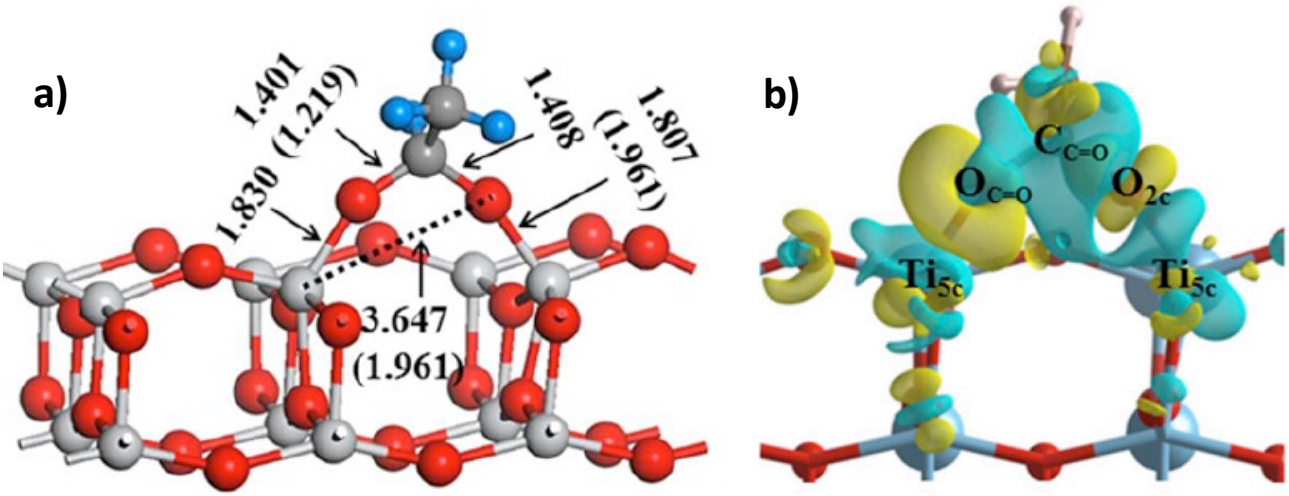
a)
1.401
(1.219)
1.830
1.408
1.807
(1.961)
3.647
(1.961)
b)
$C_{C=O}$
$O_{C=O}$
O_{2c}
Ti_{5c}
Ti_{5c}

FIGURE 5

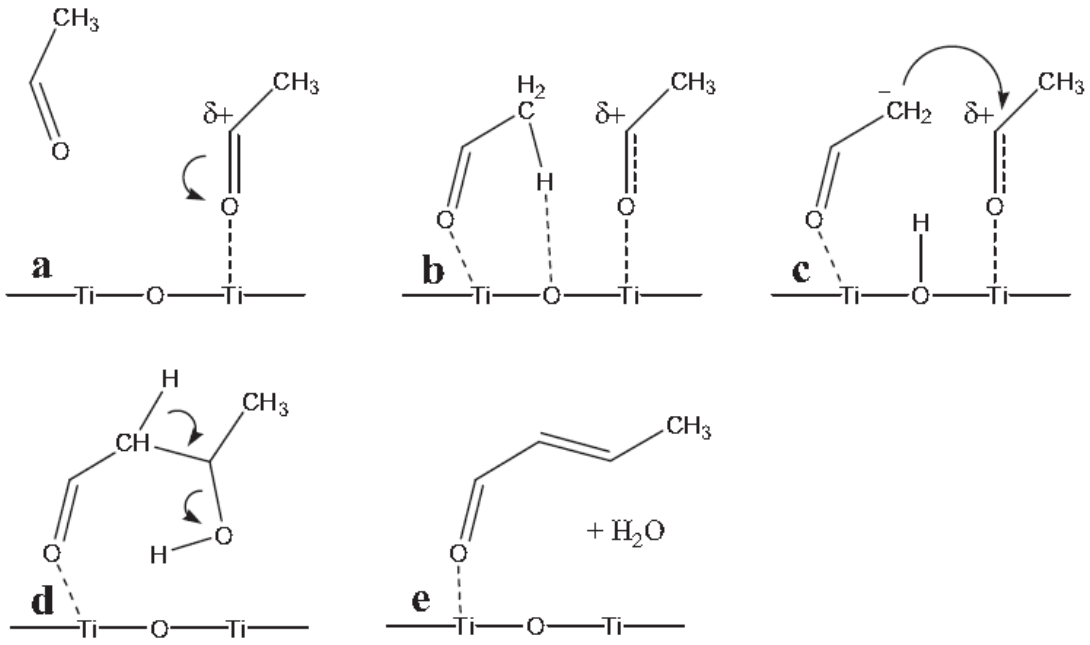
CH3
O
δ+
CH3
O
a
Ti
O
Ti
H2
C
H
O
δ+
CH3
O
b
Ti
O
Ti
CH2
δ+
CH3
O
H
O
c
Ti
O
Ti
H
CH
CH3
O
H
O
d
Ti
O
Ti
CH3
+ H2O
O
e
Ti
O
Ti

FIGURE 6

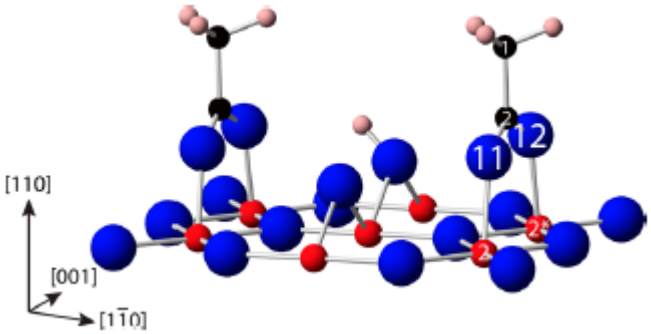

FIGURE 7

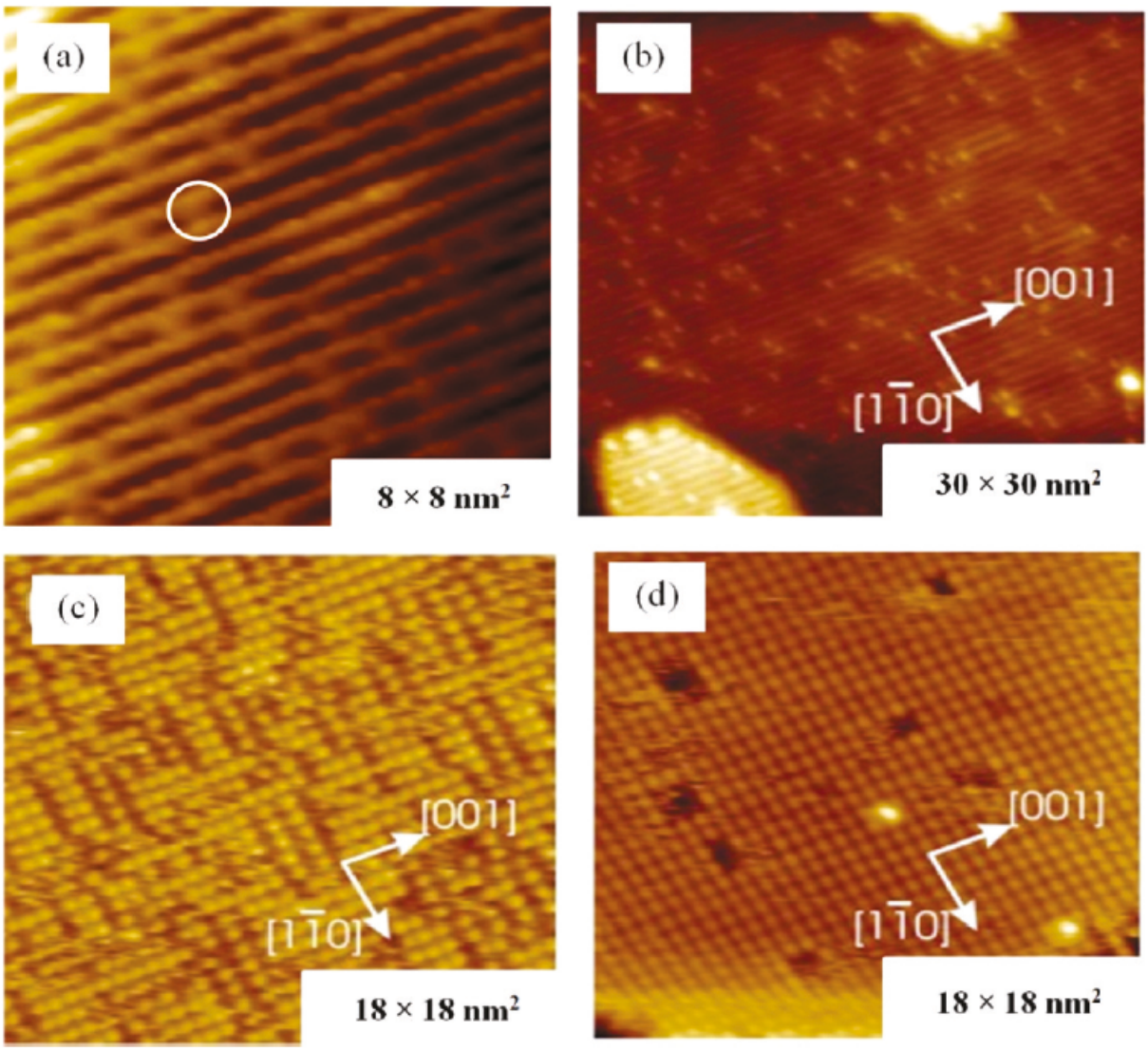
(a)
8 × 8 nm²
(b)
[001]
[1$\bar{1}$0]
30 × 30 nm²
(c)
[001]
[1$\bar{1}$0]
18 × 18 nm²
(d)
[001]
[1$\bar{1}$0]
18 × 18 nm²

FIGURE 8

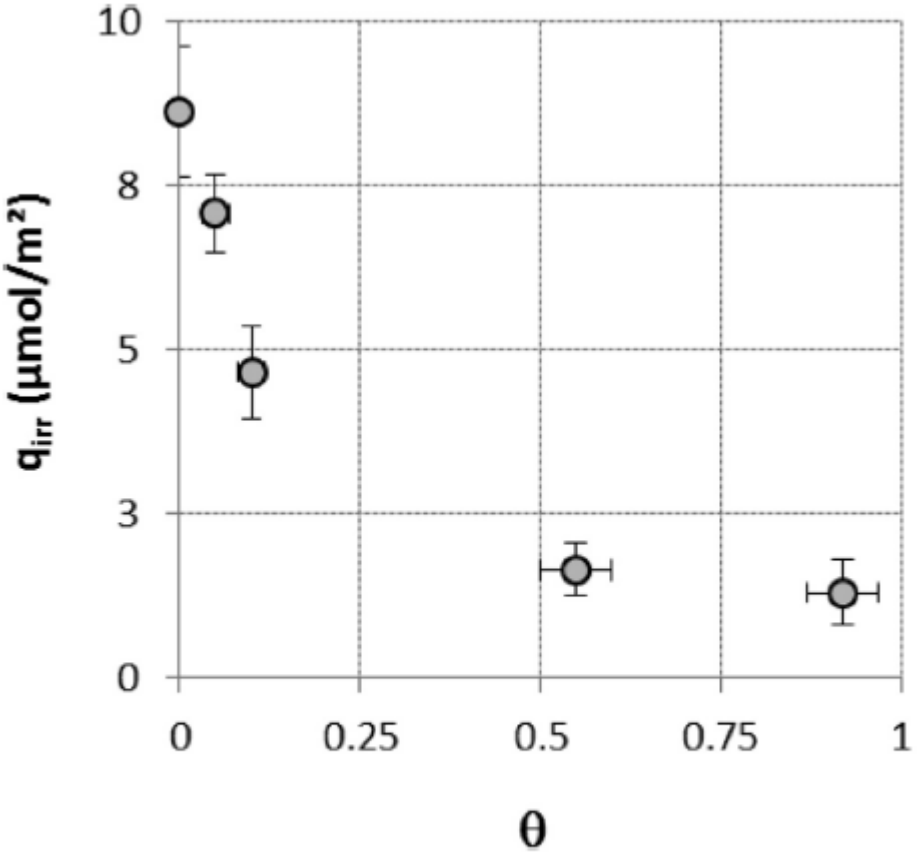

FIGURE 9

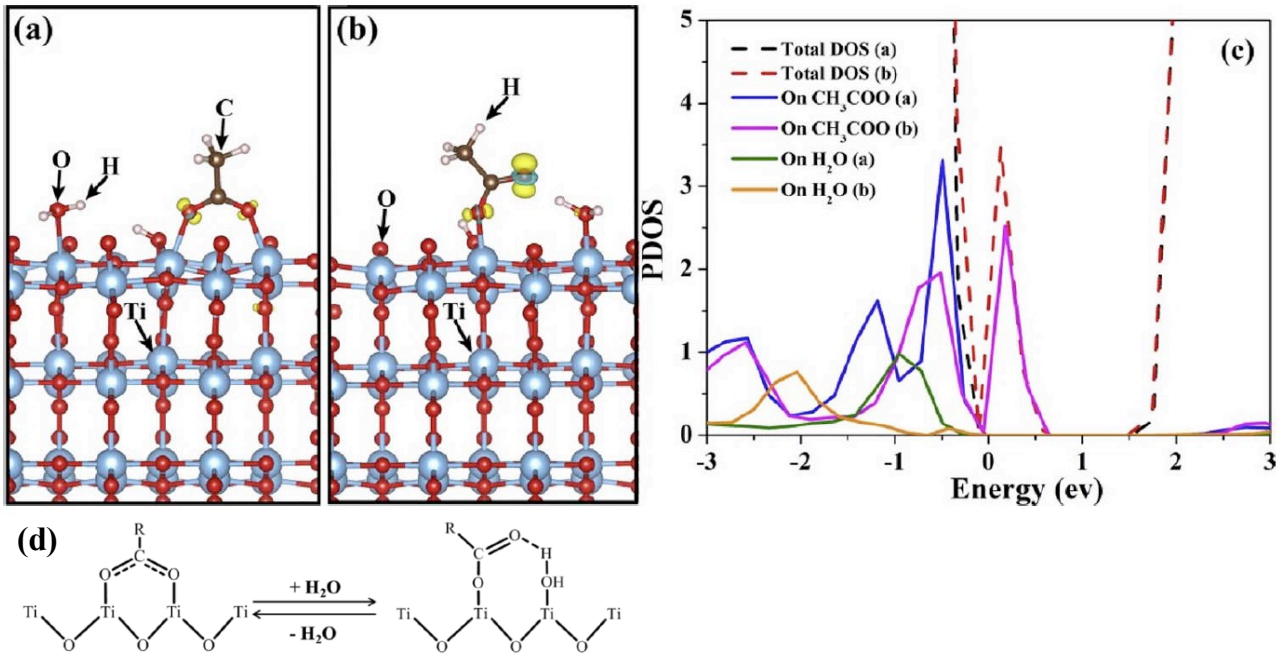
(a)
(b)
(c)
(d)
C
O
H
Ti
H
O
Ti
Total DOS (a)
Total DOS (b)
On CH3COO (a)
On CH3COO (b)
On H2O (a)
On H2O (b)
PDOS
Energy (ev)
+ H2O
- H2O

FIGURE 10

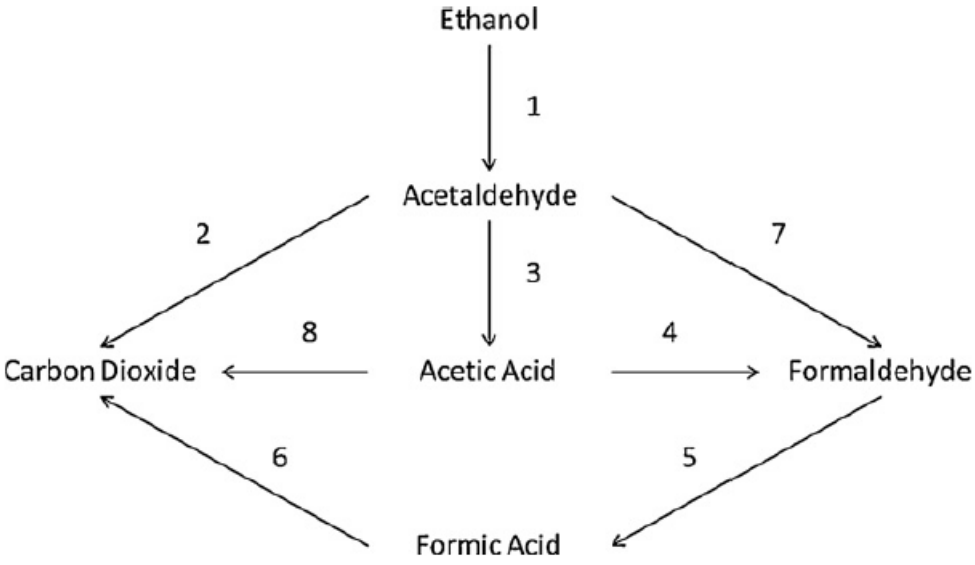
Ethanol
1
Acetaldehyde
2
3
7
8
4
Carbon Dioxide
Acetic Acid
Formaldehyde
6
5
Formic Acid

FIGURE 11

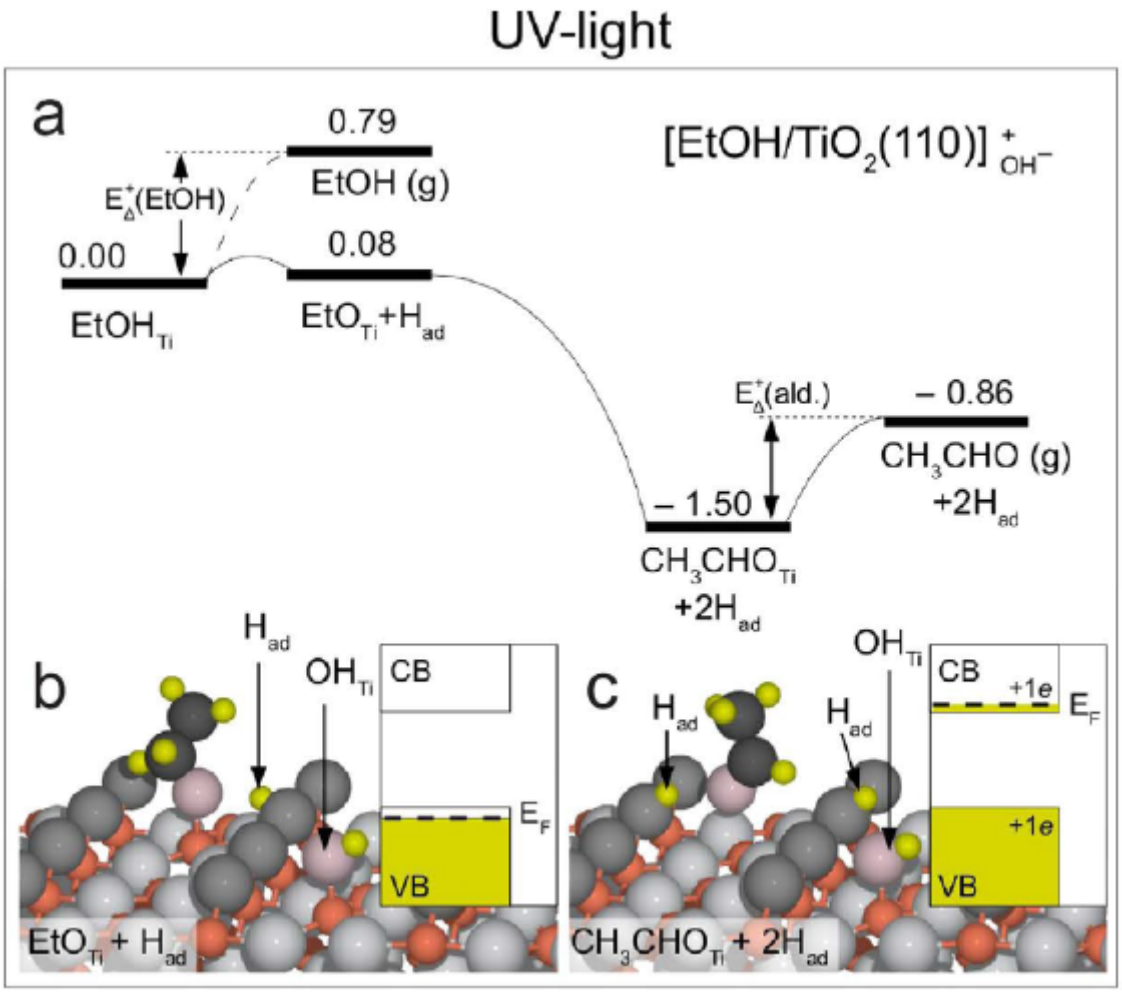
UV-light
a
0.79
EtOH (g)
[EtOH/TiO2(110)] +OH−
E*Δ(EtOH)
0.00
EtOHTi
0.08
EtOTi+Had
E*Δ(ald.)
– 0.86
CH3CHO (g)
+2Had
– 1.50
CH3CHOTi
+2Had
b
Had
OHTi
CB
EF
VB
EtOTi + Had
c
Had
Had
OHTi
CB
+1e
EF
+1e
VB
CH3CHOTi + 2Had

FIGURE 12

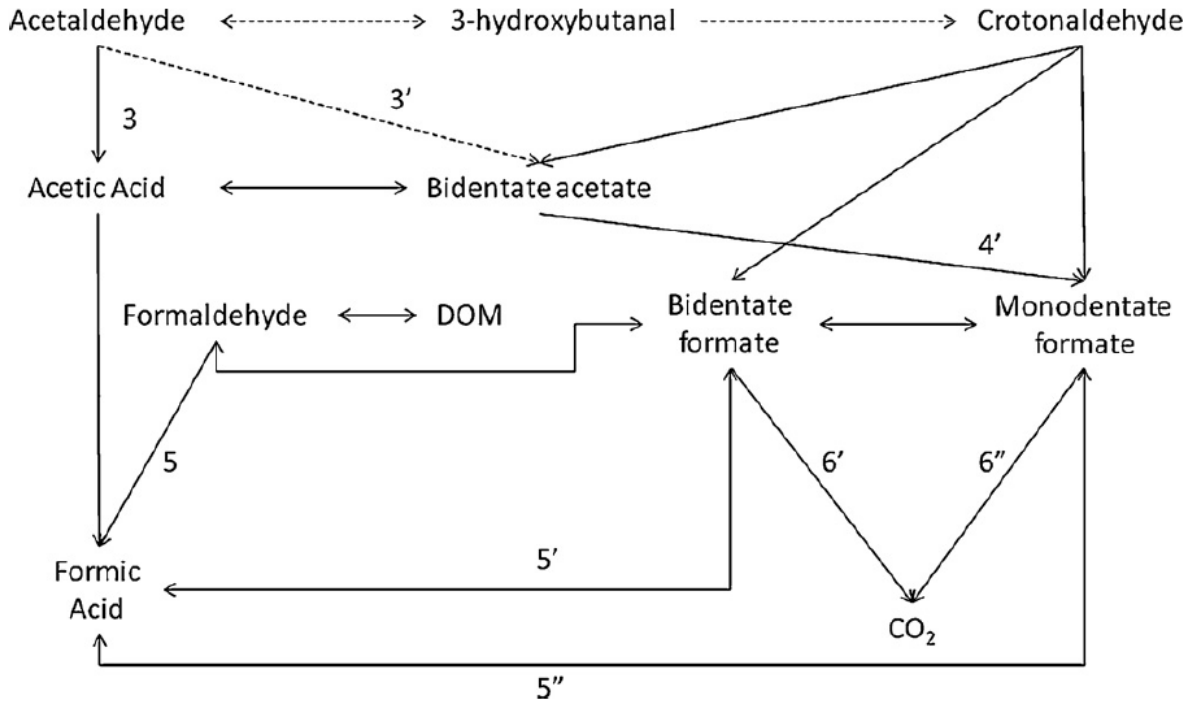
Acetaldehyde
3-hydroxybutanal
Crotonaldehyde
3
3'
Acetic Acid
Bidentate acetate
4'
Formaldehyde
DOM
Bidentate formate
Monodentate formate
5
6'
6"
5'
Formic Acid
CO_2
5"

FIGURE 13

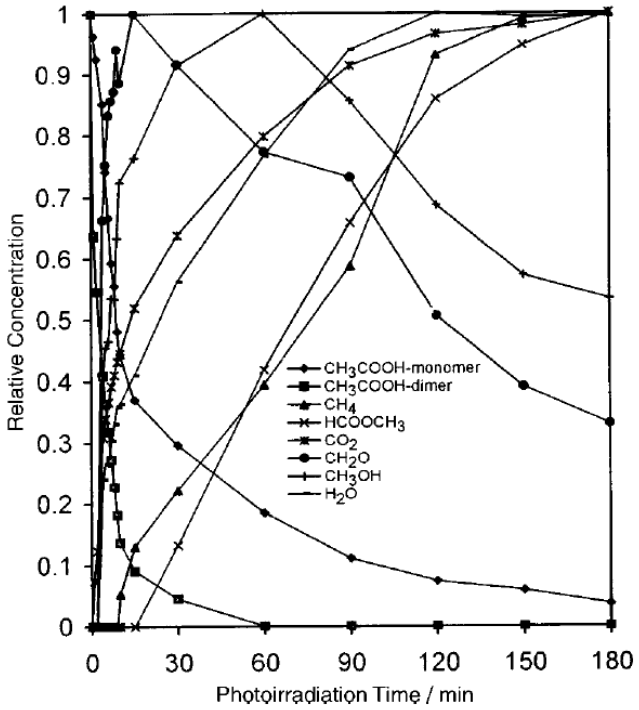

$$CH_3COOH + h^+ \rightarrow CH_3^{\cdot} + CO_2 + H^+$$

$$H^+ + O_2^- \rightarrow {}^{\cdot}OOH$$

$$CH_3^{\cdot} + O_2 \rightarrow CH_3OO^{\cdot}$$

$$CH_3OO^{\cdot} + {}^{\cdot}OOH \rightarrow CH_3OOOOH$$

$$CH_3OOOOH + CH_3COOH \rightarrow CH_3OH + CH_2O + O_2 + CO_2$$

FIGURE 14

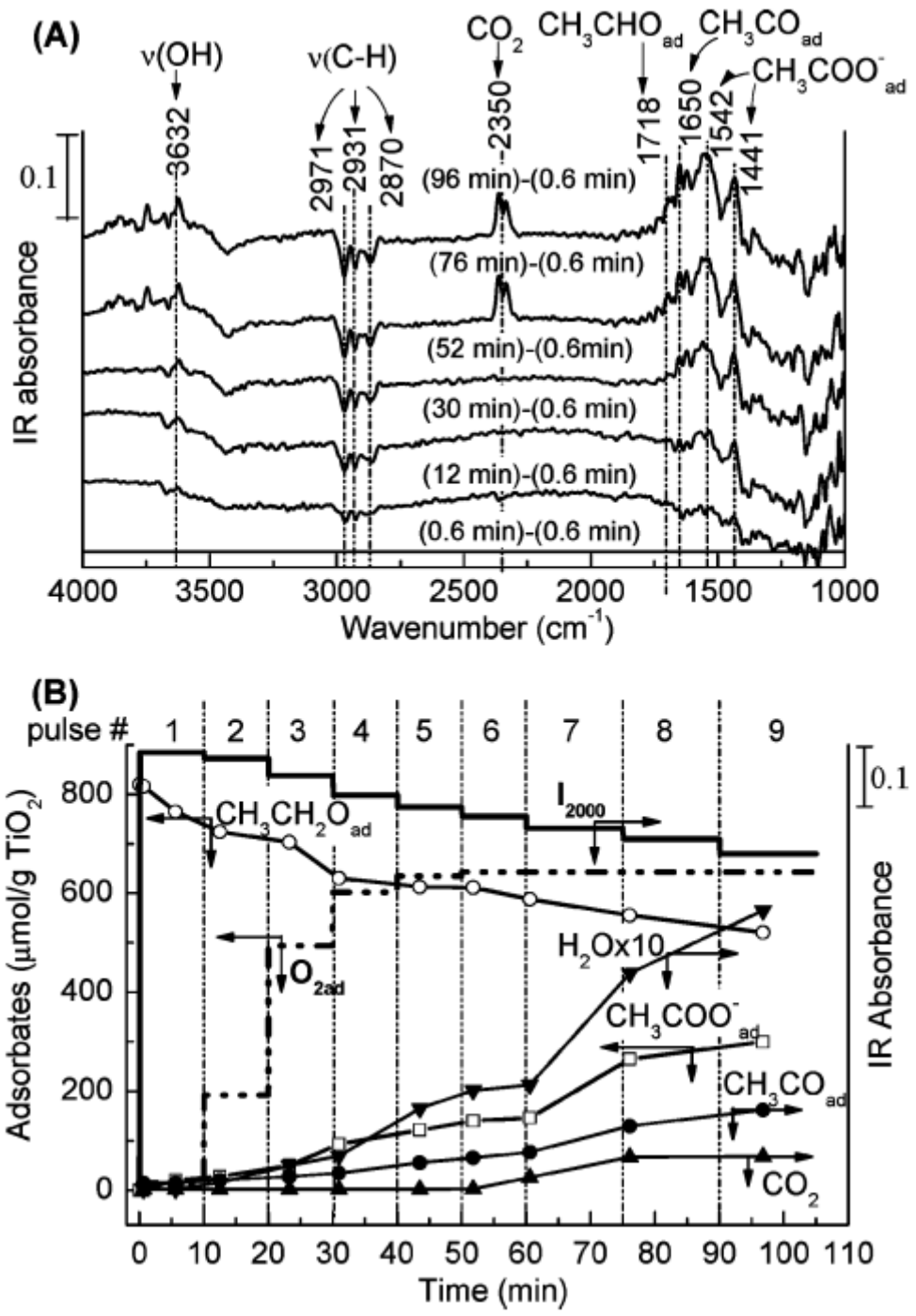
(A)
ν(OH)
ν(C-H)
CO2
CH3CHOad
CH3COad
CH3COO-ad
3632
2971
2931
2870
2350
1718
1650
1542
1441
0.1
(96 min)-(0.6 min)
(76 min)-(0.6 min)
(52 min)-(0.6min)
(30 min)-(0.6 min)
(12 min)-(0.6 min)
(0.6 min)-(0.6 min)
IR absorbance
4000 3500 3000 2500 2000 1500 1000
Wavenumber (cm-1)
(B)
pulse # 1 2 3 4 5 6 7 8 9
Adsorbates (μmol/g TiO2)
800 600 400 200 0
CH3CH2Oad
I2000
O2ad
H2Ox10
CH3COO-ad
CH3COad
CO2
0.1
IR Absorbance
0 10 20 30 40 50 60 70 80 90 100 110
Time (min)

FIGURE 15

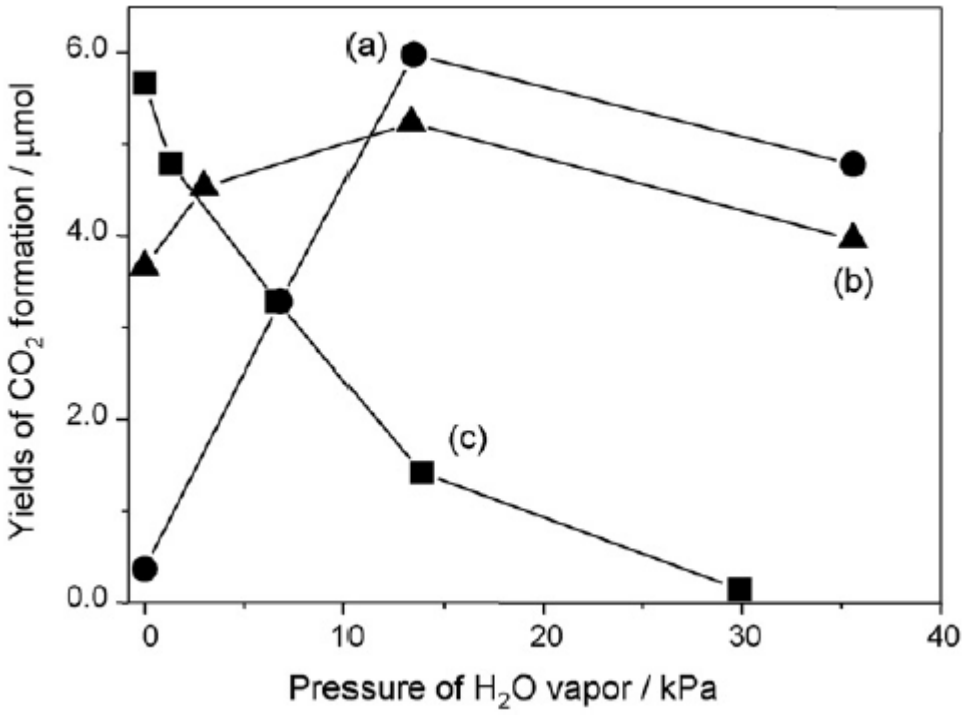
6.0
4.0
2.0
0.0
0
10
20
30
40
(a)
(b)
(c)
Yields of CO_2 formation / µmol
Pressure of H_2O vapor / kPa

FIGURE 16

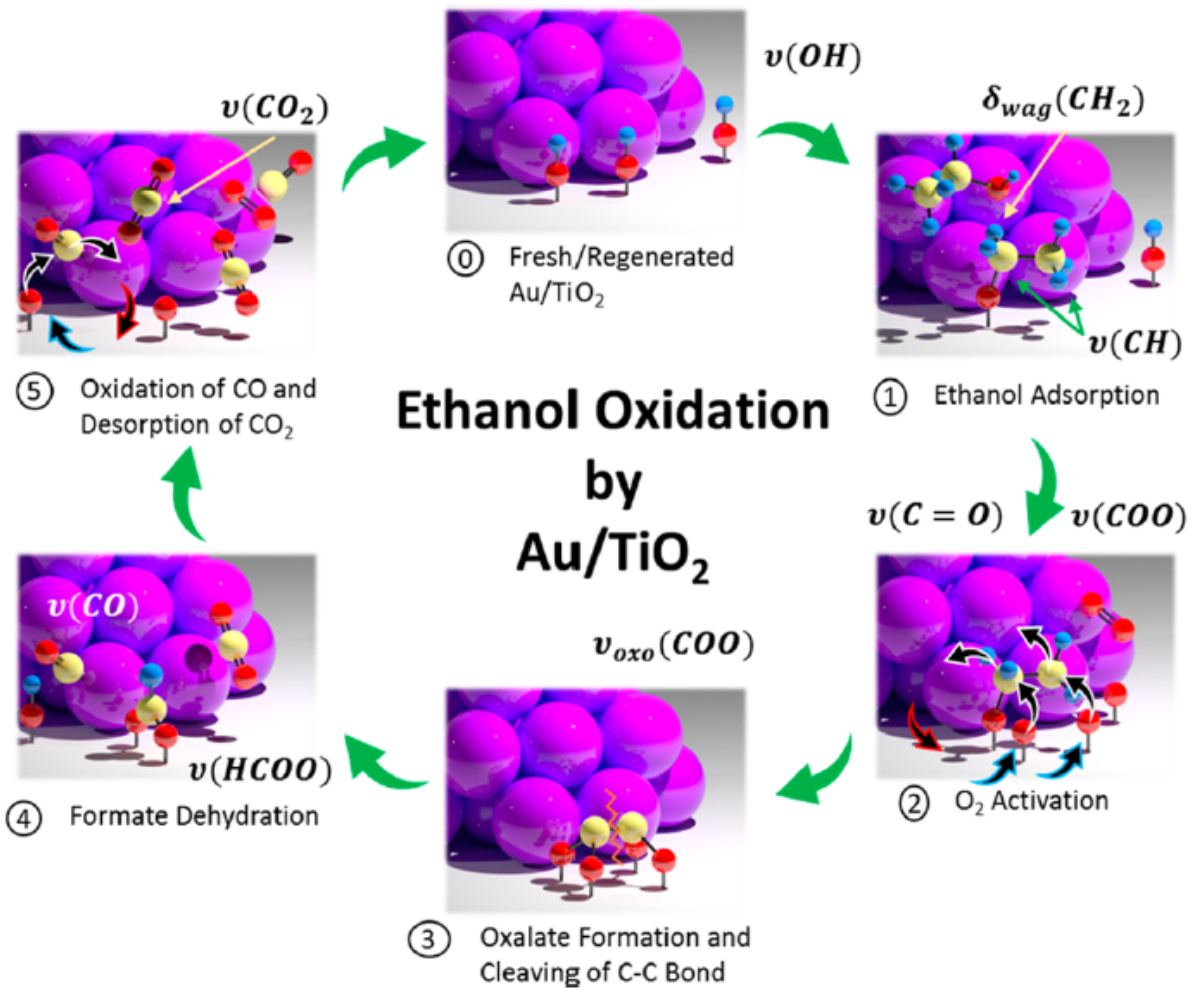
Ethanol Oxidation by Au/TiO2
0 Fresh/Regenerated Au/TiO2
v(OH)
δwag(CH2)
v(CH)
1 Ethanol Adsorption
v(C = O)
v(COO)
2 O2 Activation
voxo(COO)
3 Oxalate Formation and Cleaving of C-C Bond
v(CO)
v(HCOO)
4 Formate Dehydration
v(CO2)
5 Oxidation of CO and Desorption of CO2

FIGURE 17

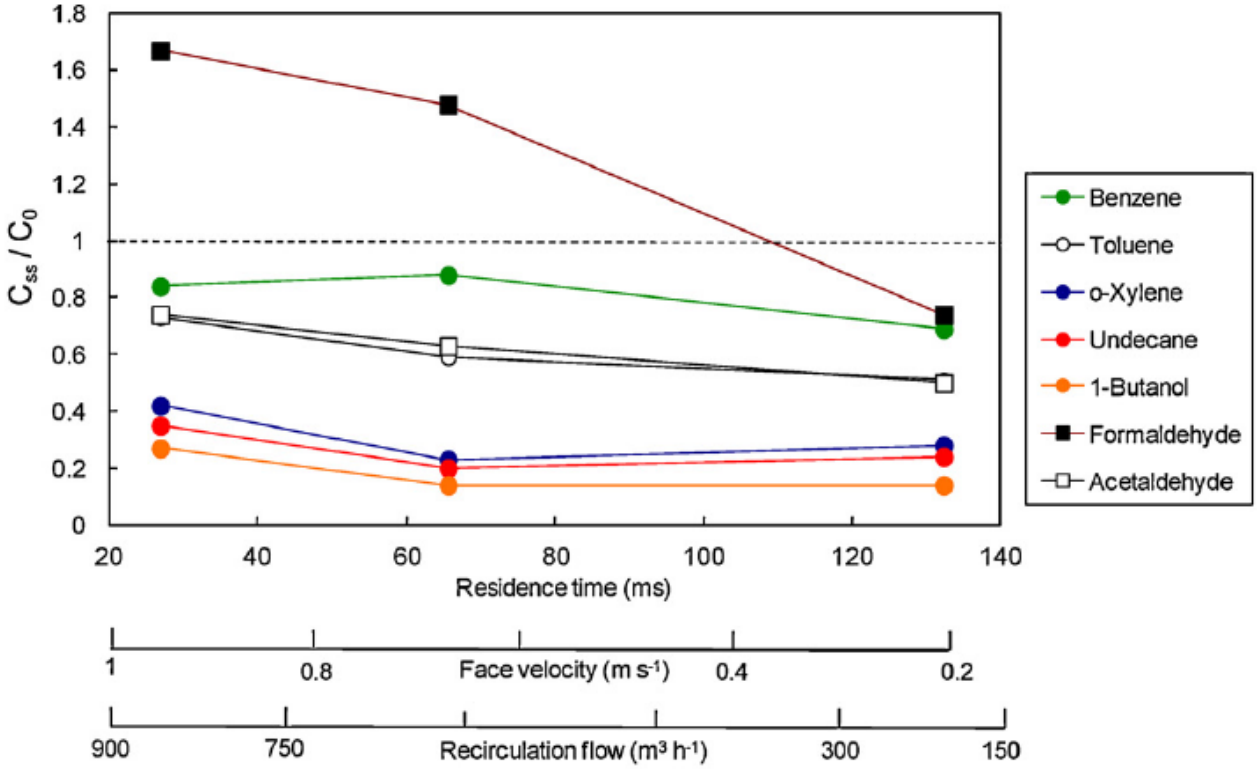
1.8
1.6
1.4
1.2
1
0.8
0.6
0.4
0.2
0
C_{ss} / C_0
20
40
60
80
100
120
140
Residence time (ms)
Benzene
Toluene
o-Xylene
Undecane
1-Butanol
Formaldehyde
Acetaldehyde
1
0.8
Face velocity (m s-1)
0.4
0.2
900
750
Recirculation flow (m3 h-1)
300
150

FIGURE 18

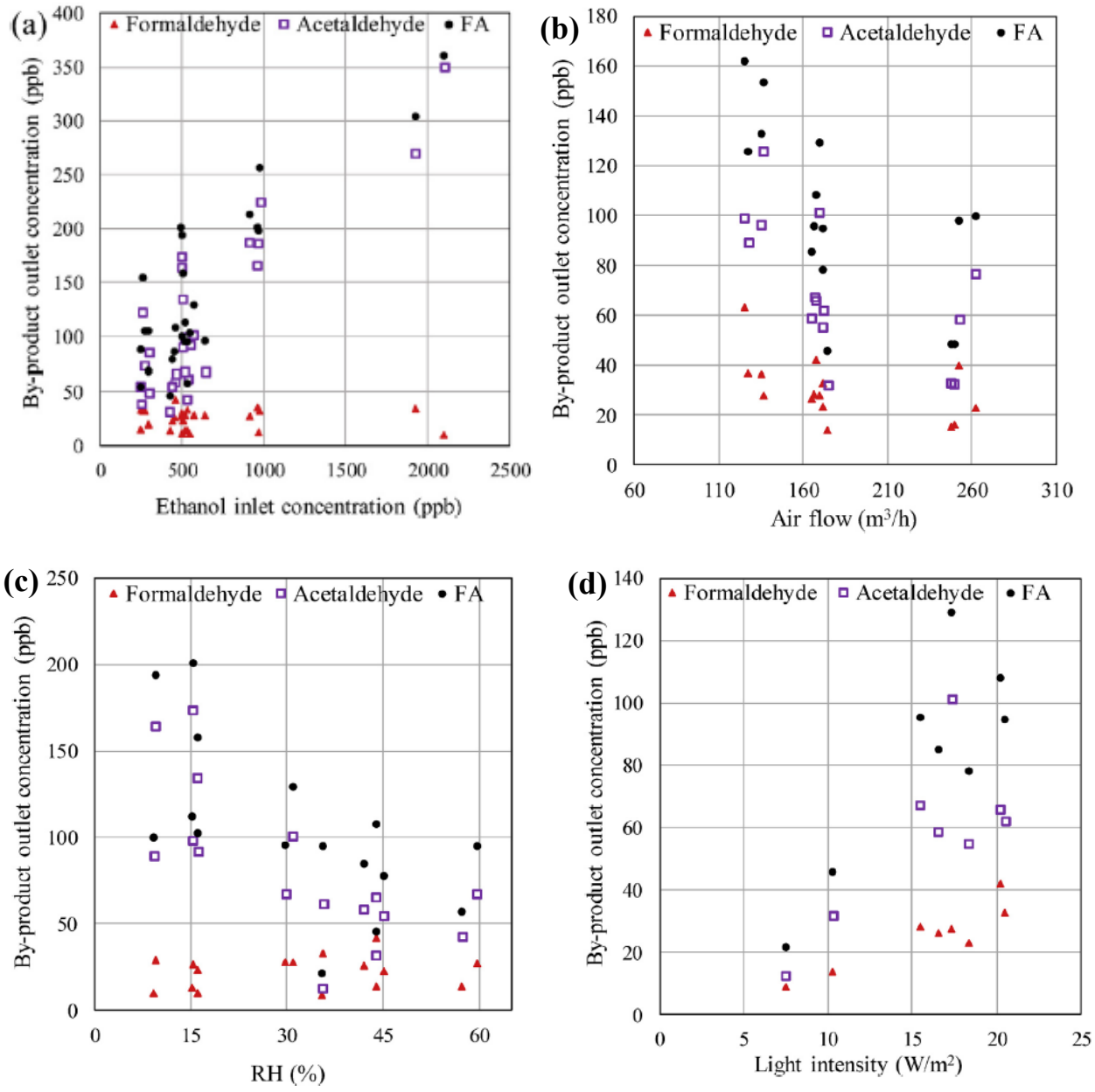
(a)
Formaldehyde
Acetaldehyde
FA
By-product outlet concentration (ppb)
Ethanol inlet concentration (ppb)
(b)
Air flow (m³/h)
(c)
RH (%)
(d)
Light intensity (W/m²)

FIGURE 19

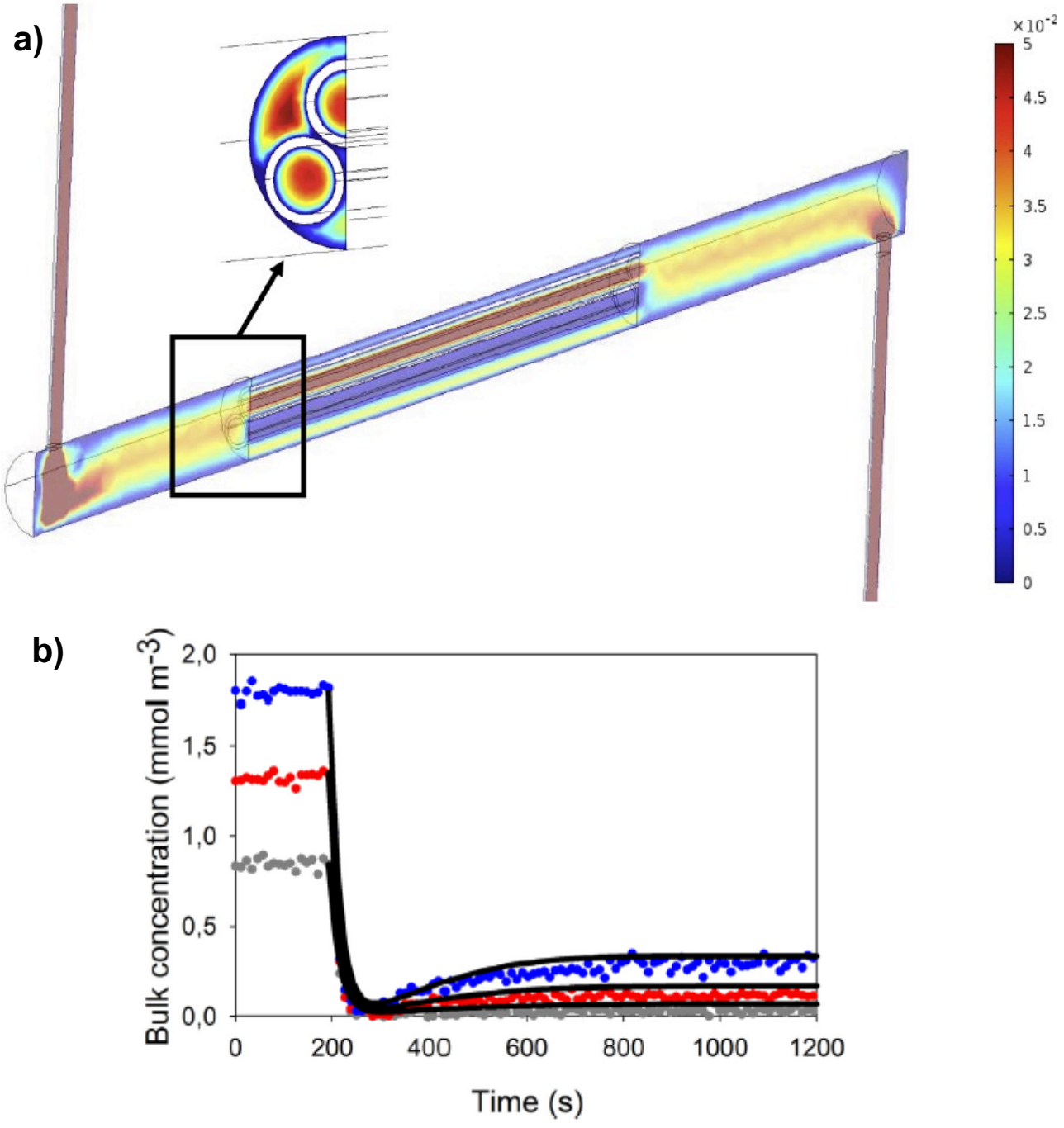
a)
×10-2
5
4.5
4
3.5
3
2.5
2
1.5
1
0.5
0
b)
Bulk concentration (mmol m-3)
2,0
1,5
1,0
0,5
0,0
0
200
400
600
800
1000
1200
Time (s)

FIGURE 20

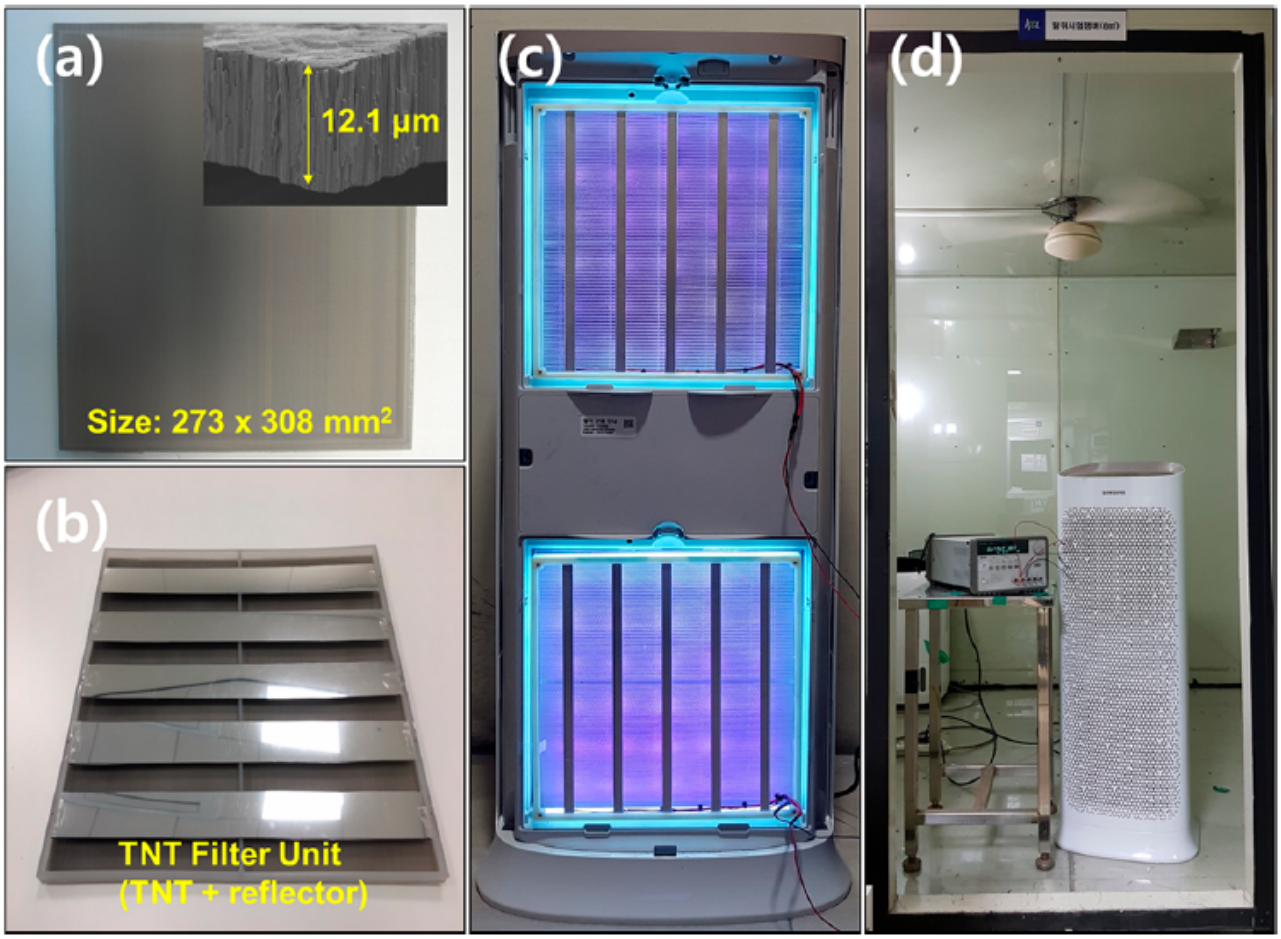

FIGURE 21